MASTERARBEIT | MASTER'S THESIS

Titel | Title

Investigating Aneuploidy in the Small Intestine using “mini guts”

verfasst von | submitted by

Leonie Drakos BSc

angestrebter akademischer Grad | in partial fulfilment of the requirements for the degree of

Master of Science (MSc)

Wien | Vienna, 2025

Studienkennzahl lt. Studienblatt | Degree programme code as it appears on the student record sheet:	UA 066 865
Studienrichtung lt. Studienblatt | Degree programme as it appears on the student record sheet:	Masterstudium Molecular Biology
Betreut von | Supervisor:	Ass.-Prof. Stephanie Ellis BSc PhD

Abstract

The maintenance of tissue homeostasis relies on surveillance mechanisms that ensure chromosomes are equally segregated during mitosis. However, errors can occur that result in aberrant karyotypes, a phenotype known as aneuploidy. Aneuploidy is rarely observed in healthy somatic tissues due to its detrimental effects on cellular growth and viability. Nevertheless, the fate and survival of aneuploid cells varies depending on tissue and physiological context. Cell nonautonomous mechanisms that act to recognize and eliminate aneuploid cells have been hinted at in the developing mammalian embryo. In contrast, persistent aneuploid cells are a clinical hallmark of many tumour types. Intriguingly, both aneuploidy and susceptibility to tumorigenesis are increased in the colon compared to the small intestine raising the prospect of enhanced aneuploidy-sensing mechanisms in the small intestine. In this thesis, we aim to test this possibility by developing new protocols to induce and study aneuploidy in small intestinal organoids. Specifically, we use the mitotic assembly checkpoint inhibitor Reversine to trigger aneuploidy during organoid morphogenesis, without compromising organoid growth and viability. Following implementation of our optimized treatment regime, we detect the presence of aneuploid cells via immunofluorescence. Our data suggests upregulation of p53 and cleaved caspase 3 in Reversine-treated enteroid monolayers. We propose p53-mediated apoptosis as a possible protective mechanism for aneuploid cell removal from the tissue. Our technical advances set the stage for further study of the local tissue response that acts to limit the growth of aneuploid cells, thus preserving homeostasis, in the intestinal epithelium.

Zusammenfassung

Die Aufrechterhaltung der Gewebehomöostase beruht auf Überwachungsmechanismen, welche sicherstellen, dass Chromosomen während der Mitose gleichmäßig aufgetrennt werden. Dennoch können Fehler auftreten, die zu abnormalen Karyotypen führen, ein Phänotyp bekannt als Aneuploidie. Aneuploidie tritt in gesunden, somatischen Geweben selten auf, da sie mit schädlichen Effekten auf Zellwachstum und Lebensfähigkeit einhergeht. Schicksal und Überleben aneuploider Zellen sind abhängig von Gewebe- und physiologischem Kontext. Es wird vermutet, dass Zell-autonome Mechanismen für die Erkennung und Eliminierung aneuploider Zellen in sich entwickelnden Säugetierembryos verantwortlich sind. Gegensätzlich dazu ist das Bestehen von aneuploiden Zellen als Kennziechen vieler Tumore. Verglichen mit dem Dünndarm sind Aneuploidie und Tumorigeneseanfälligkeit erhöht im Dickdarm, dies lässt auf einen verbesserten Erkennungsmechanismus von aneuploiden Zellen im Dünndarm schließen. In dieser Arbeit wollen wir diese Möglichkeit testen, indem wir neue Protokolle zur Induktion und Untersuchung von Aneuploidie in Dünndarm-Organoiden entwickeln. Im Detail werden wir den mitotischen Checkpunkt Inhibitor Reversine benutzen, um Aneuploidie während Organoid-Morphogenese auszulösen, ohne dabei Organoidwachstum und Überlebensfähigkeit zu beinträchtigen. Im Anschluss an unser optimiertes Reversine-Behandlungs-Regiment, wurden aneuploide Zellen mit Hilfe von Immunfluoreszenz detektiert. Unsere Daten deuten darauf hin, dass p53 and cleaved caspase 3 in Reversine-behandelten Enteroid Monolayers hoch reguliert sind. Wir schlagen die p53-vermittelte Apoptose als möglichen Schutzmechanismus für die Entfernung aneuploider Zellen aus dem Gewebe vor. Unsere technischen Fortschritte legen die Grundlage für weitere Untersuchungen der lokalen Gewebereaktion, die das Wachstum aneuploider Zellen begrenzt und so die Homöostase im Darmepithel bewahrt.

Acknowledgements

First and foremost, I would like to express my sincere gratitude to Stephanie for providing me with the opportunity to establish and work on the organoid project. By entrusting me with this project, you enabled me to gain valuable experience in both setting up new systems and refining existing protocols as well as gaining scientific insides in the world of small intestinal organoids.

Secondly, I cannot express how thankful I am for the unwavering support and guidance provided by Sanskriti. Although not initially involved in this project, you consistently went above and beyond to help resolve challenges, tirelessly pushing experiments forward through researching for and with me. Beyond your exceptional role as a supervisor and mentor, you have also become a great friend—one whose always just fun to talk to (your stories are hilarious) but also gives great life advice and emotional support.

I would like to thank the entire Ellis lab, as well as its former members, for their great support. In particular, Eleni, I truly appreciate how you always made time to listen to my struggles, offering invaluable advice and practical solutions. It was also a pleasure to have spontaneous conversations with you about everything and anything. Clara, I thoroughly enjoyed our Tissue-Culture sessions, where we could discuss a wide range of topics, and your thoughtful advice was always on point. Leonie S., sharing a desk space with you was a highlight—I deeply valued our conversations that ventured beyond the lab, and your company made the workspace so much more enjoyable. Miki, starting this Master's journey alongside you has been great: I could really benefit from your help and knowledge and obviously enjoyed the daily conversations with you. Of course, I have to mention that your support during my Push-up challenge was also greatly appreciated. Ameya, thank you for the insightful imaging advice you provided. I also want to thank Almedina and Andreea who were always fun to talk to.

Lastly, I want to express my gratitude for my family and friends for their support and encouragement throughout my studies.

Table of contents

1 Introduction

In this work we focus on studying the fate of aneuploid cells and the underlying mechanisms within the small intestine using intestinal organoids and 2D enteroid monolayers. In this introduction, I will firstly discuss aneuploidy and its effects across different tissues. Next, I will illustrate the morphology, function and cell composition of the intestine with particular focus on the differences between the colon and the small intestine. Then, a short explanation on how we plan to introduce aneuploidy will be followed by an introduction of our model systems and finally the research goals of this thesis will be summarized.

Aneuploidy

Epithelial tissues exhibit high cellular turnover throughout life while maintaining homeostasis, this requires a balance between cell proliferation and cell elimination. Mitosis, the process of cell division, is tightly controlled, ensuring equal segregation of DNA into two daughter cells. Multiple surveillance mechanisms are in place to prevent mis-segregation of chromosomes, that could result in aneuploidy (Barnum & O'Connell, 2014; Guillot & Lecuit, 2013).

The term aneuploidy refers to cells that have either gained or lost chromosomes or chromosomal regions, leading to an abnormal karyotype (Holland & Cleveland, 2012; Johnson et al., 2024; Lukow et al., 2021; Santaguida et al., 2017; Santaguida & Amon, 2015). Aneuploidy can be further divided into numerical and structural; the former describes the failed distribution of whole chromosomes and the latter portrays large changes (deletions, inversions, translocation, etc.) within individual chromosomes (Ben-David & Amon, 2020). Aneuploidy and chromosomal instability (CIN) are closely correlated; however, they are not identical terms. CIN refers to a high and continuous rate of errors during chromosomal segregation, which can eventually lead to aneuploidy. It is classified as a form of genomic instability. Therefore, aneuploidy denotes the end-product of CIN. While CIN inevitably leads to aneuploidy, the opposite is not always the case. As a matter of fact, aneuploid cell lines exist, that remain chromosomally stable with no ongoing display of chromosomal instability (Ben-David & Amon, 2020; Siri et al., 2021). Nevertheless, recent data shows that the relationship between aneuploidy and CIN might be more complex and suggests that aneuploidy itself can cause CIN (Garribba et al., 2023).

Despite the stringent controls during cell division that act to ensure faithful DNA segregation, mistakes can sometimes still occur, potentially leading to aneuploidy. The sources of aneuploidy can be categorized into 1) mitotic checkpoint defects, 2) merotelic chromosome attachment, 3) cohesin-dependent defects, 4) centrosome amplification.

1) Mitotic checkpoint defects

The mitotic checkpoint, also referred to as spindle assembly checkpoint (SAC), consists of multiple protein components such as MAD1, MAD2, BUB1, BUBR1 (=MAD3), BUB3 (=BUB1B) and CENP-E that form a signalling network (Holland & Cleveland, 2012; Sansregret & Swanton, 2017). The SAC gets activated at the beginning of mitosis and will only be deactivated once all kinetochores (= protein structures assembled at the centromere region of the chromosomes) are properly attached to microtubules emanating from opposite spindle poles. For cells to leave mitosis and progress to anaphase, SAC signalling needs to be turned off, allowing segregation of chromosomes (Baker et al., 2005; Lara-Gonzalez et al., 2021; McAinsh & Kops, 2023).

Unattached kinetochores will facilitate the recruitment and binding of SAC proteins, ultimately forming the mitotic checkpoint complex (MCC). Active SAC halts the cell cycle by inhibiting the action of anaphase promoting complex/cyclosome (APC/C), which once activated facilitates sister-chromatid separation. Only the correct attachment of microtubules to kinetochore will displace SAC proteins, allowing APC/C to become active and anaphase to happen. Importantly, MPS1 is a spindle assembly checkpoint kinase, responsible for the recruitment of multiple MCC components and its proper function is crucial for the inhibitory function of the SAC (Lara-Gonzalez et al., 2021; McAinsh & Kops, 2023). Complete loss of SAC proteins is embryonically lethal in mammals, while heterogenous mutations in individual SAC components can lead to increased levels of aneuploid cells (Holland & Cleveland, 2012; Sansregret & Swanton, 2017; Santaguida & Amon, 2015).

2) Merotelic attached chromosomes

Although the SAC provides a stringent surveillance mechanism, chromosomes that have one single kinetochore connected to both spindle poles (termed merotelic attachment) escape its control since they fulfill the SAC inactivation requirement. Even though most of the merotelic chromosomes will be successfully segregated, some of them can get locked into the cleavage furrow, leading to DNA damage following cytokinesis. Others get excluded from the main nucleus forming a micronucleus, which can be segregated correctly or mis-segregated between the two daughter cells. Both scenarios might result in chromosomal rearrangements caused by possible DNA damage in micronuclei. A possible cause of merotelic chromosomes are perturbed microtubules dynamics: Correction of improperly attached microtubules to kinetochores can only be achieved by microtubule depolymerization and re-attachment, however this process might continue to be erroneous if microtubule dynamics are perturbed potentially eliciting aneuploidy (Holland & Cleveland, 2012; Sansregret & Swanton, 2017).

3) Cohesin dependent defects

Another source of CIN are mutations in the cohesin complex. Cohesin typically keeps sister chromatids joined together during mitosis. While most cohesin is removed along the length of the chromosomes in prophase, removal of centromeric cohesion is only permitted in anaphase. This ensures faithful chromosome segregation and if impaired, can cause pre-mature sister-chromatid separation, possibly leading to aneuploid daughter cells (Holland & Cleveland, 2012; Sansregret & Swanton, 2017).

4) Centrosome duplication

Finally, chromosomal mis-segregation can be caused by centrosome duplication. Duplicated centrosomes can lead to multipolar divisions which cause massive segregation errors and are incompatible with viable daughter cells. Cells try to cope with centrosome multiplication by attempting to aggregate all centrosomes into two poles, thereby creating a “pseudo” bi-polar spindle. However, this approach might also lead to increased CIN, as it has the risk of creating merotelic chromosome attachments (Holland & Cleveland, 2012; Levine et al., 2017; Sansregret & Swanton, 2017).

On a cellular level, abnormal karyotypes induce massive changes in gene dosage. Consequently, the cell must deal with more proteins and protein subunits in unbalanced stoichiometric ratios, surpassing the workload protein quality control pathways can handle, leading to proteotoxic stress. Furthermore, aneuploid cells are known to undergo metabolic adaptation and often upregulate transcripts involved in stress responses. They can also display increased levels of DNA damage and

impaired proliferation. It is perhaps not surprising that aneuploid cells often get eliminated by apoptosis (Garribba et al., 2023; Knouse et al., 2014; Lukow et al., 2021; Santaguida et al., 2017; Santaguida & Amon, 2015). In fact, it has been reported that some mammalian cell types upregulate p53, a transcription factor ensuring genome integrity, and undergo p53-mediated cell arrest as a mechanism to cope with chromosomal segregation errors (Johnson et al., 2024; Knouse et al., 2014; Narkar et al., 2021; Santaguida et al., 2017; Santaguida & Amon, 2015).

In development, aneuploidy is often embryonically lethal and aneuploid cells are extremely rare in somatic tissues. In fact, studies investigating the role of aneuploid cells during murine embryonic development revealed aneuploidy-induced embryos fail to develop post-implantation. However, chimeric embryos consisting of aneuploid and euploid cells, show increased removal of aneuploid cells prior to implantation via apoptosis and slowed cell cycles. The presence of enough euploid cells within the chimeric embryo can rescue the phenotype (Bolton et al., 2016). After implantation p53-mediated autophagy is thought to eliminate aneuploid cells, enabling viable embryo development. Furthermore, higher proliferation in remaining euploid cells compensates for reduction in overall cell numbers caused by the removal of aneuploid cells. This compensatory proliferation mechanism allows to achieve similar total cell numbers in aneuploid chimeric embryos when compared to the euploid control embryos (Singla et al., 2020). While in the embryo the robust removal of aneuploid cells is well characterized and indicates the presence of a tissue wide-sensing mechanism, little is known about adult tissues.

Previous papers proposed that tissues with high turnover rates such as the intestine, the skin and blood contain less aneuploid cells while their presence is higher in less proliferating tissues like the liver or the brain (Knouse et al., 2014). However, a recent study indicates that even in the liver and brain, aneuploidy levels are rather low at a level of approximately 5% (Knouse et al., 2014; Santaguida et al., 2017; Santaguida & Amon, 2015). Intriguingly, the consistently low levels of aneuploidy observed across different tissues indicates the presence of a potential tissue-wide mechanism eliminating aneuploid cells, particularly in tissues with lower turnover rates, where abnormal cells are not constantly removed.

Interestingly around 90% of solid tumors and 50% of blood cancers display a high degree of aneuploidy. At first glance, this observation is rather counterintuitive since chromosomal instability is generally associated with a fitness disadvantage. However, in the context of cancer, the increased rate of CIN can lead to copy number changes of cancer driver genes and facilitates a higher diversity of karyotypes, fuelling tumor evolution. Moreover, a high degree of CIN is often correlated with immune evasion, poor patient prognosis, therapy resistance and metastasis promotion (Ben-David & Amon, 2020; Hoevenaar et al., 2020; Knouse et al., 2014; Santaguida et al., 2017). While aneuploidy promotes tumorigenesis in some tissues, it might be inhibitory in others, highlighting the importance of tissue context and cell type (Ben-David & Amon, 2020; Santaguida et al., 2017). Recent studies in the *Drosophila* gut showed that induction of aneuploidy in intestinal stem cells, increases their proliferation, leading to dysplasia formation (Brás et al., 2021). If a tumor had already been initiated in the tissue, the additional burden of aneuploidy enhanced tumorigenesis even more (Brás et al., 2021). In other *Drosophila* tissues, such as the primordial wing disc, aneuploid epithelial cells are ultimately eliminated from the disc (Joy et al., 2024). Elegant genetic studies in the *Drosophila* wing disc suggest that aneuploid cells are sensed on the basis of ribosome gene dose changes; cells harbouring aneuploidies that do not impact ribosomal gene copy number are not eliminated (Ji et al., 2021). Cell-type and tissue-specific responses are once more highlighted when comparing monolayer cultures of RPE-1 (retinal pigmental epithelial) or HCT116 (human colon carcinoma) cells that upon chromosome mis-segregation upregulate p53 consequently leading to cell cycle arrest.

Mouse colon organoids or human mammary organoids on the other hand do not upregulate p53 and show no proliferation defect, despite harbouring aneuploid cells. Further experiments demonstrated that HCT116 cells, cultured in Matrigel to resemble a 3D culture, upregulated p53 and underwent cell cycle arrest similarly to the 2D HCT116 monolayer culture when confronted with aneuploidy. This indicates that tissue architecture on its own might not account for the different responses to aneuploidy. Instead, these findings highlight how the role of aneuploidy is very tissue context-dependent (Marques & Kops, 2023; Narkar et al., 2021).

The importance of the varying effects of aneuploidy within different tissues becomes even more apparent when looking at the intestinal tract; while small intestinal cancers are relatively scarce, colorectal cancers (CRCs) are more common, especially in humans (Barsouk et al., 2019) and CRCs are very often correlated with high levels of CIN and aneuploidy (Garribba et al., 2023; Hoevenaar et al., 2020). Mouse studies have shown that when high levels of chromosomal instability were introduced in both, the small intestine and the colon, which shared the same genetic make-up, massive adenoma formation was observed only in the colon (Hoevenaar et al., 2020). Researchers have shown that disrupting the SAC component BubR1, in combination with a constitutively active mutation in the tumor suppressor gene *Apc*, leads to greater tumor formation in the colon compared to the small intestine. This difference in tumor susceptibility between the two tissues highlights the importance of understanding aneuploid consequences across different tissues (C. V. Rao et al., 2005). As a side note, the emergence of CRC can be influenced by multiple factors beyond aneuploidy. Therefore, when discussing differences in tumor incidence between the small and large intestine, the different microbiome compositions and immune landscape have to be mentioned. In fact the microbiome of the colon is thought to influence tumorigenesis and cancer development (Ağagündüz et al., 2023; Keku et al., 2015). While these factors are worth exploring, we will not focus on their effects in this work.

Having pointed out the varying effects of aneuploidy across different tissues, as well as showcasing different tissue-specific-mechanisms to deal with aneuploid cells, it remains to be deciphered whether aneuploid cells persist in the small intestine. Moreover, it remains to be elucidated if aneuploid cells get eliminated via cell autonomous mechanisms or if a tissue-wide, non-cell-autonomous mechanism is at play in the intestine.

The murine intestine

Different regions of the intestine respond differently to similar levels of CIN, thus it is important to recognize the distinct differences in structure, function and cellular composition between the small intestine and the colon, despite being part of the same system. Overall, the intestine plays a crucial role in our digestive system and can be divided into two main parts: the small intestine and the large intestine or colon. Despite being part of the same system, these two structures differ significantly in both morphology and function and should thus be considered different tissues.

The innermost layer of the gastrointestinal tract is the mucosa, which comprises an epithelial layer that interfaces with the lumen. Beneath the epithelium lies the lamina propria, a layer of connective tissue that provides structural support and is essential for vascularization. The third part of the mucosa is the muscularis mucosae, a thin layer of smooth muscles that enable local movements (J. N. Rao & Wang, 2010).

The small intestine extends from the stomach ultimately connecting to the large intestine and can be anatomically subdivided in duodenum, jejunum and ileum. Its major function is the uptake of

nutrients, water and ions. Beyond facilitating the uptake of metabolites, a key function of the small intestine is to serve as a barrier, protecting the intestinal epithelium from the potentially harmful luminal environment such as mechanical stress, microorganisms and pH alterations (Gehart & Clevers, 2019; J. N. Rao & Wang, 2010).

The inner lining of the small intestine consists of a columnar epithelium that is folded, forming invaginations known as crypts and protrusions called villi. The villi significantly enhance the intestinal surface area, facilitating the efficient absorption of nutrients. However, their exposure to the intestinal lumen results in constant abrasion and loss of differentiated cells from the villus top. To counteract this, the intestinal epithelium undergoes self-renewal every 3-5 days driven by intestinal stem cells (ISC) (Clevers, 2013; Gehart & Clevers, 2019). The ISCs, marked by the expression of Lgr5 (Clevers, 2013), are located at the very base of the crypt and are termed crypt base columnar (CBC) stem cells. CBC stem cells are essential for epithelial homeostasis since they give rise to transit-amplifying progenitor (TAP) cells, which proliferate and differentiate into the four primary epithelial cell types: absorptive enterocytes (water and nutrient absorption), mucus-secreting goblet cells, antimicrobial Paneth cells and hormone-producing enteroendocrine cells. The crypts serve as specialized niches that not only house CBC stem cells but also provide a supportive microenvironment through interactions with Paneth cells which are intermingled between the stem cells, suppling epidermal growth factor (EGF), wingless-related integration site (WNT) ligands and Notch stimuli for stem cell maintenance as well as antimicrobial peptides. This arrangement ensures a continuous replenishment of epithelial cells to maintain intestinal function and facilitate repair, with CBC cells playing a crucial role in driving this regenerative process (Capdevila et al., 2024; Clevers, 2013; Gehart & Clevers, 2019; Sato & Clevers, 2012).

However, recent findings have revised our understanding of intestinal stem cell organization and function. The traditional model, which puts Lgr5+ (CBC) stem cells as the exclusive drivers of intestinal epithelial renewal, has been challenged by the identification of a distinct stem cell population in the upper crypt region (Capdevila et al., 2024; Clevers, 2013). This newly discovered cell population is transcriptionally distinct from Lgr5+ cells, displays multipotency and self-renewal capacity and can give rise to Lgr5+ cells as well as other differentiated intestinal lineages (Capdevila et al., 2024).

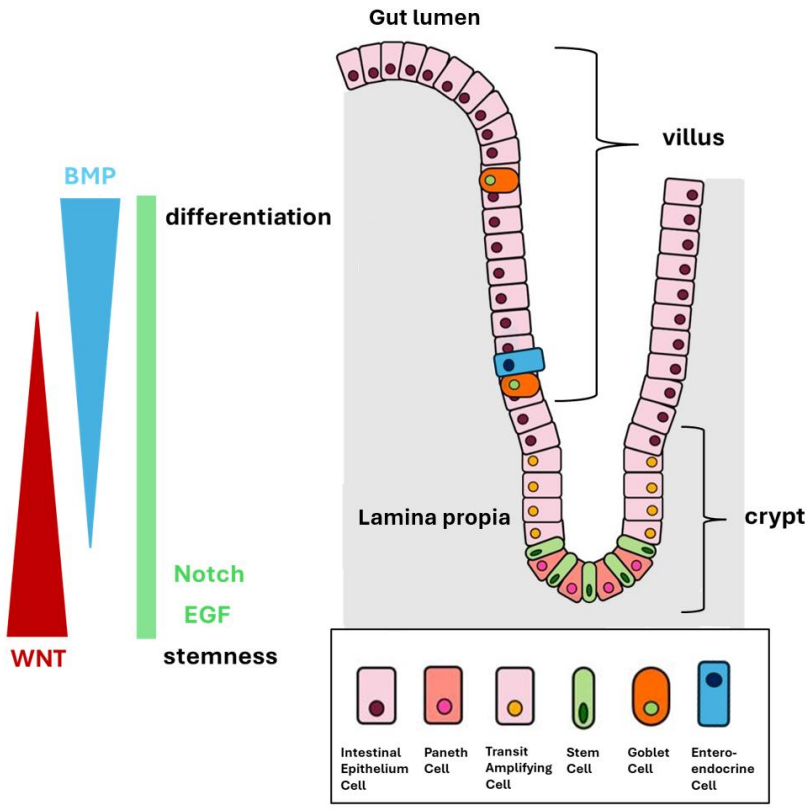

***Figure 1**: Illustration of the classical crypt- and villi-architecture of the small intestine.*

The large intestine begins at the junction with the small intestine and extends to the anus. It can be anatomically subdivided into the cecum and the colon which is also why the large intestine is often referred to as colon. It is mainly involved in water, vitamin, and electrolyte absorption as well as the transportation of feces to the rectum (Azzouz & Sharma, 2025).

Contrary to the small intestine, the large intestinal epithelium does not contain any villi and forms a rather flat surface, housing crypts (Barker et al., 2007; Gehart & Clevers, 2019; Širvinskas et al., 2022). These crypts are lined with a columnar epithelium similarly to the small intestine. At the crypt' base Lgr5+ CBC stem cells can be found, whose role is to replenish the pool of differentiated intestinal cells by giving rise to transit amplifying cells (TAC). TAC, differentiate into absorptive colonocytes or secretory cells like goblet cells and enteroendocrine cells (Širvinskas et al., 2022). Rather than Paneth cells, deep secretory cells (DSCs) are interspersed between the intestinal stem cells at the base of the crypt and provide essential niche factors for maintaining stemness (Gehart & Clevers, 2019; Sasaki et al., 2016).

Despite being both essential parts of the digestive system and sharing certain characteristics, the large intestine and small intestine display significant differences in morphology, cell types and function and should not be considered equivalent tissues. This should especially be considered when designing new experiments.

Introducing aneuploidy: Reversine and its role

In most somatic tissues aneuploid cells are relatively rare, which makes studying their fate and consequences particularly difficult (Ben-David & Amon, 2020; Knouse et al., 2014; Santaguida &

Amon, 2015). Methods to artificially introduce chromosome mis-segregation in the system of interest provide an important tool to investigate behaviour and characteristics of aneuploid cells.

Over the years, multiple strategies to induce aneuploidy have emerged: There is a mouse model carrying a mutation in the SAC gene *Bub1b* (Knouse et al., 2014), whose function is required to ensure correct chromosome segregation. Other models overexpress MAD2, another component of the SAC, which causes mitotic delay and aneuploidy (He et al., 2018; Sotillo et al., 2007). Also, different strategies make use of chemical MPS1-inhibitors, such as NMS-P715 (Narkar et al., 2021) or Reversine (Johnson et al., 2024), which override the SAC. The antimitotic drug Nocodozole can cause deploymerization of spindle-microtubules leading to a prolonged cell cycle. After drug washout, the emergence of merotelic chromosome attachments results in lagging chromosomes (Cimini et al., 2001; He et al., 2018). Overexpression of PLK4, a kinase involved in centriole duplication, leads to centrosome amplification and ultimately aneuploidy (Garvey et al., 2021; Levine et al., 2017).

Given the various methods of aneuploidy induction, we opted in this study to use Reversine, as it has been shown to induce aneuploidy in multiple different cell lines (He et al., 2018; Narkar et al., 2021; Santaguida et al., 2017), as well as in mouse and human colonoids (Johnson et al., 2024; Narkar et al., 2021). Other research groups, utilized Reversine to trigger chromosome mis-segregation in mouse embryos (Bolton et al., 2016; Singla et al., 2020). Lastly, other drugs delay mitosis by interfering with microtubules dynamics, causing p53 mediated G1-arrest independent of chromosomal mis-segregation (Santaguida et al., 2017). We opted for Reversine, since it overrules the SAC instead of arresting the cell cycle completely and offers a rather fast approach to induce aneuploidy. Additionally, its prior successful usage in colonoids showed its applicability in intestinal models.

Reversine functions by inhibiting the catalytic activity of the MPS1 kinase, which is crucial for proper regulation of the SAC. As described earlier, the SAC is a stringent surveillance mechanism governing correct kinetochore-microtubule attachment by halting cell cycle progression until faithful attachments are achieved. By inhibiting MPS1 function, the SAC gets overruled and even cells with improperly attached chromosomes get segregated thereby increasing the possibility of aneuploidy. Improperly attached chromosomes include monotelic attachments, where one chromosome is attached to only one spindle pole; syntelic attachments, describing two microtubules from the same spindle pole are connected to the same chromosome; and merotelic attachments, generated when one sister chromatid is attached to microtubules emanating from two opposite spindle poles (Lara-Gonzalez et al., 2021; McAinsh & Kops, 2023).

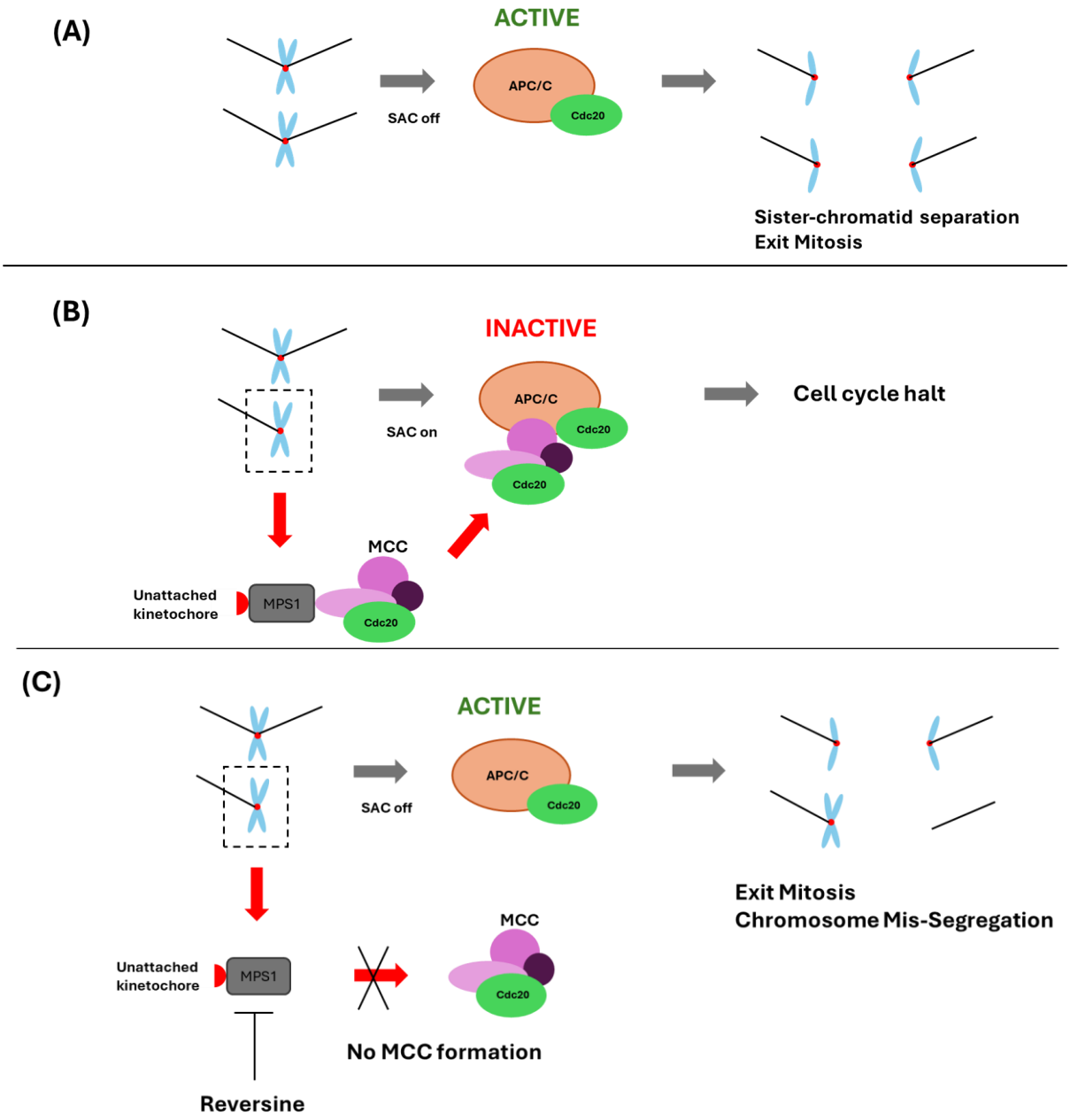

***Figure 2*: The function MPS-1 inhibitor Reversine. (A)** *amphitelic attached chromosomes, SAC is off, Mitosis can progress,* **(B)** *unattached kinetochore activates the SAC, cell cycle hold,* **(C)** *unattached kinetochore in the presence of Reversine, SAC is off, cell cycle progresses leading to chromosomal mis-segregation. MCC = mitotic checkpoint complex (MAD2, BUBR1, BUB3 + CDC20). Kinetochore: red dots.*

Model system: murine small intestinal organoids

Organoids are *in vitro* cell culture systems composed of three-dimensional structures that self-organize through spatially restricted lineage commitment. Those structures contain the key differentiated cell types, characteristic of a specific organ, thereby recapitulating the structure and the function of the organ *in vivo*. Organoids are commonly generated using either induced

pluripotent stem cells (iPSCs), embryonic stem cells (ESCs) or stem cells isolated directly from primary tissue (Almeqdadi et al., 2019; Corrò et al., 2020).

In 2009, Toshiro Sato and Hans Clevers established the first intestinal organoid, by culturing individual stem cells or entire crypts from the small intestine in Matrigel. Matrigel is primarily composed of laminin and collagen IV, forming a basement membrane-like matrix. By supplying those stem cells with growth factors (Noggin, R-spondin-1, EGF) that are normally found in the intestinal stem cell niche they were able to culture small intestinal organoids (Almeqdadi et al., 2019; Corrò et al., 2020; Sato et al., 2009). Later, Sato and colleagues could additionally establish organoids from the colon, termed colonoids (Sato et al., 2011).

Since then, an immense number of studies has demonstrated the value of using organoid stem cell models, showcasing their broad applicability. Organoids offer a high-throughput and versatile tool for studying infectious diseases, conducting drug screens, and gaining insights into fundamental biological processes to mention a few (Almeqdadi et al., 2019). In this project, we aim to use organoids to explore the effects of aneuploidy induction in the small intestine.

Despite being a well-established and utilized biological tool, we miss crucial insights regarding the proliferative capacity of organoids at each day of culture. This becomes particularly important when designing experimental regimes, such as Reversine-treatment, that must specifically target cycling cells to achieve their desired effect. The success of any Reversine-based strategy to induce aneuploidy directly depends on the number of cycling cells present during the treatment window.

Enteroid Monolayers: from 3D to 2D

While organoids serve as an effective *in vitro* 3D model that recapitulates both the function and morphology of the intestine, their complex structure presents challenges. Specifically, tracking individual cells within the intact 3-dimensional tissue is difficult, a problem that becomes even more evident when high-resolution tracking and quantification of individual cells—such as aneuploid cells —are required (Thorne et al., 2018).

In recent years, establishing the enteroid monolayers has been successfully accomplished. These 2D structures are generated from isolated crypts, either directly obtained from the intestine or derived from intestinal organoid cultures, and cultured on a flat, Matrigel-coated surface in typical ENR (EGF, Noggin, R-spondin-1) media (Altay et al., 2019; Li et al., 2020; Ordóñez-Morán, 2020; Thorne et al., 2018). It has been shown that enteroid monolayers self-organize into distinctive regions: proliferative zones resembling a crypt-like structure and differentiated zones mimicking villi-like structures. Moreover, these systems are capable of self-renewal, establish stereotypical apical-basal polarization and consist of the key intestinal cell types (Altay et al., 2019; Thorne et al., 2018).

In conclusion, 2D enteroid monolayers provide a high-throughput system for studying behaviour of individual cells within the context of the intestine, which will equip us with a system to study the effects of Reversine on individual cells.

Goals of the Thesis

Despite the extensive research on aneuploidy, its consequence in adult tissues is poorly understood. In particular, the mechanisms by which the small intestine and large intestine recognizes and copes with aneuploid cells as they arise are not characterized. The long-term objective of this project is to exploit the tractability of intestinal organoid systems to shed light on this critical, clinically relevant knowledge gap. However, experimental models to induce and study aneuploidy in small intestinal

organoids are currently lacking. Therefore, the goal of this thesis project was to develop such a model, thus setting the stage for further research to understand tissue-level mechanisms that underlie death or survival of aneuploid, chromosomally unstable cells that arise in the small intestine.

Specifically, this work addresses the following aspects:

- Characterization of cell proliferation in small intestinal organoids (critical to guide subsequent protocol optimization)
- Optimization and validation of a Reversine-based protocol to induce aneuploidy in mouse small intestinal organoids
- Characterization of cell proliferation dynamics in 2D Enteroid Monolayers
- Characterization and validation of the 2D Enteroid Monolayer treated with Reversine

Overall, this study aims to enhance our understanding on the proliferative capacity of small intestinal organoids and to establish a model system for investigating and quantifying the fate of aneuploid cells, utilizing the anti-mitotic drug Reversine.

2 Results

2.1 Establishment of the small intestinal organoid system

Small intestinal organoids have become a widely used tool to study various biological aspects. Since our lab has not previously established murine small intestinal organoids, our first goal was to set up this system, following the protocol of Sato and Clevers (2012).

Briefly, intestinal organoids are derived from primary intestinal tissue by isolating stem cell containing crypts and culturing them in Matrigel, together with media supplemented with growth factors and other molecular cues that instruct stem cell behaviour (see Methods). Contingent on media composition, crypt-derived stem cells self-organize and form 3D-organoids that recapitulate the structure of the intestine to a high degree (Sato et al., 2009; Sato & Clevers, 2012). The crypt regions, housing stem cells, are positive for olfactomedin-4 (OLFM4) which serves as an alternative marker to Lgr5+ stem cells at the base of the crypt (Flier et al., 2009; Thorne et al., 2018). Once the culture is established, organoids can be passaged indefinitely and isolation from additional primary tissue is not required.

Based on these previously published protocols, we successfully managed to establish the 3D organoid system in our laboratory (***Figure 3***). We assessed morphological changes of the organoid culture as well as the presence of OLFM4 which was visualized by immunofluorescence staining and confocal microscopy of our organoids.

In our hands, organoids could typically be maintained in culture for up to 7 days before passaging was required as indicated by the formation of a dark necrotic core that resembles the lumen of the intestine *in vivo*. Importantly, the population of organoids displayed a high degree of heterogeneity regarding morphology and growth-status after passaging (***Fig. 3***). This heterogeneity resulted from the passaging process, which breaks old organoids into smaller pieces, releasing dead cells and generating organoid fragments. The fragments that harbour intestinal stem cells have regenerative potential, and subsequently can give rise to new organoid structures. Over the period of several days, spheroids as depicted in ***Figure 3A*** initiate the process of bud formation, resulting in protrusions of crypt-containing buds from the organoid surface (***Fig. 3, B-M***). However, due to the heterogeneity that arises post-splitting, other organoid-fragments already containing some buds and therefore displaying a “more mature” phenotype, were found (***Fig. 3C***). Those fragments initiated further bud formation as well (***Fig. 3, E, F***). As illustrated in ***Figure 3, F-I***, mature organoid structures exhibiting multiple buds develop starting from day 2 and latest at day 3 of culture. By day 4 post-passage, the emergence of a necrotic core was first observed in more mature organoids (***Fig. 2, K, N, O***). By day 6, a majority of organoids possessed a prominent necrotic core, necessitating passaging shortly thereafter (***Fig. 3, P-R***). The OLFM4 expression was visible in the crypt regions of the organoids (***Fig. 4***). No OLFM4 protein could be detected in the lumen of the organoids (***Fig. 4 A-C***). A closer look at individual crypts, confirmed that OLFM4 was more enriched at the very tip of the crypts, where stem cells were located (***Fig. 4d-f***). It is important to mention that this time-course, and all other experiments we conducted, were performed with organoids that had been passaged at least twice following isolation of crypts from the intact intestine.

Overall, this data demonstrates that we successfully established the organoid system in our lab. In our hands, the organoids undergo the morphological changes of a growing organoid culture and still possess culture-maintaining stem cells, marked by OLFM4.

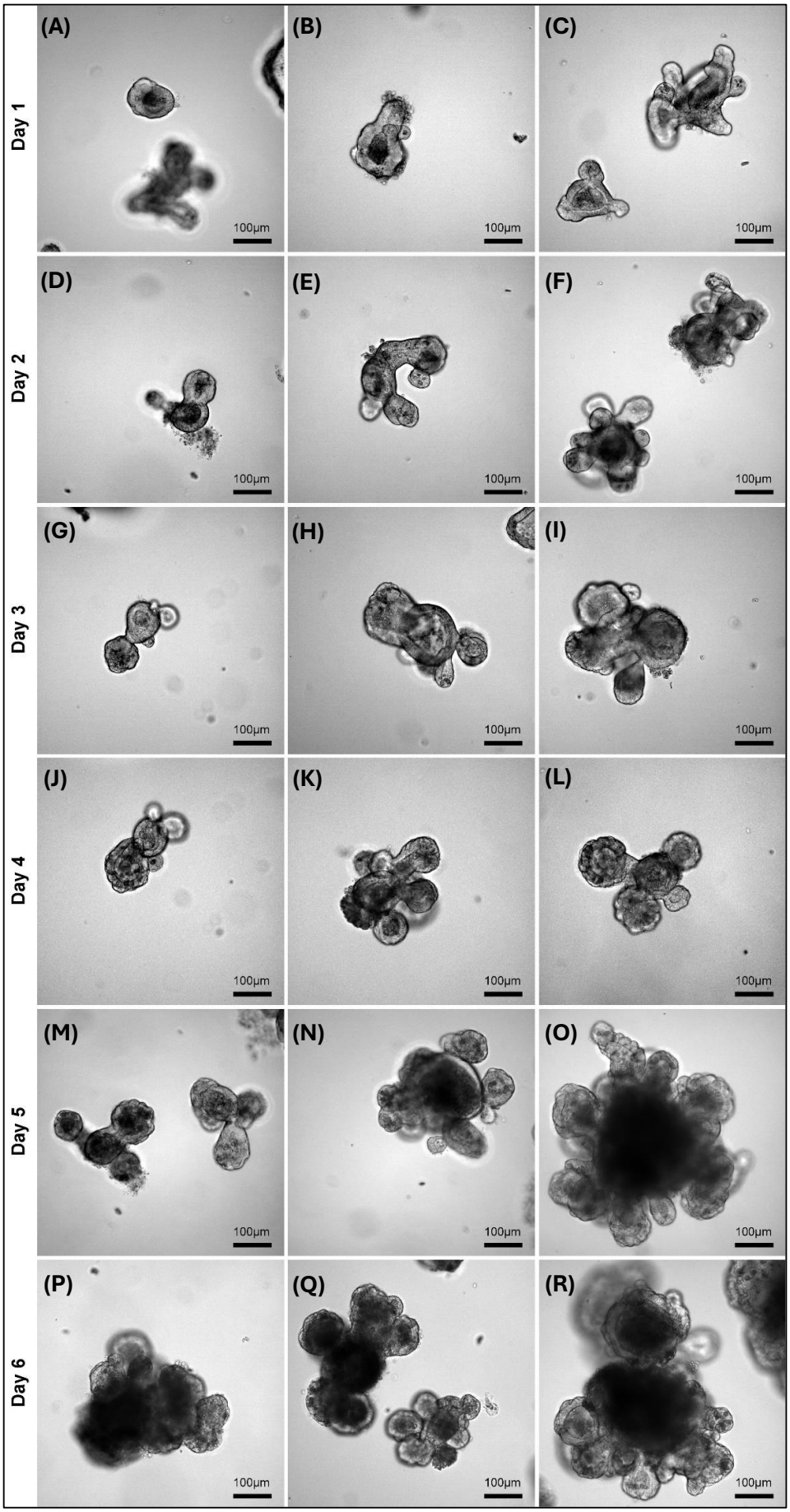
Day 1
Day 2
Day 3
Day 4
Day 5
Day 6
(A)
(B)
(C)
(D)
(E)
(F)
(G)
(H)
(I)
(J)
(K)
(L)
(M)
(N)
(O)
(P)
(Q)
(R)
100μm

***Figure 3**: **Time course of small intestinal organoids** over a period of 6 days. Each row contains 3 representative images of organoids from each of the 6 days. **(A -C**) Day 1, **(D-F)** Day 2, **(G-I)** Day 3, **(J-L)** Day 4, **(M-O)** Day 5, **(P-R)** Day 6. Brightfield images, 20x objective.*

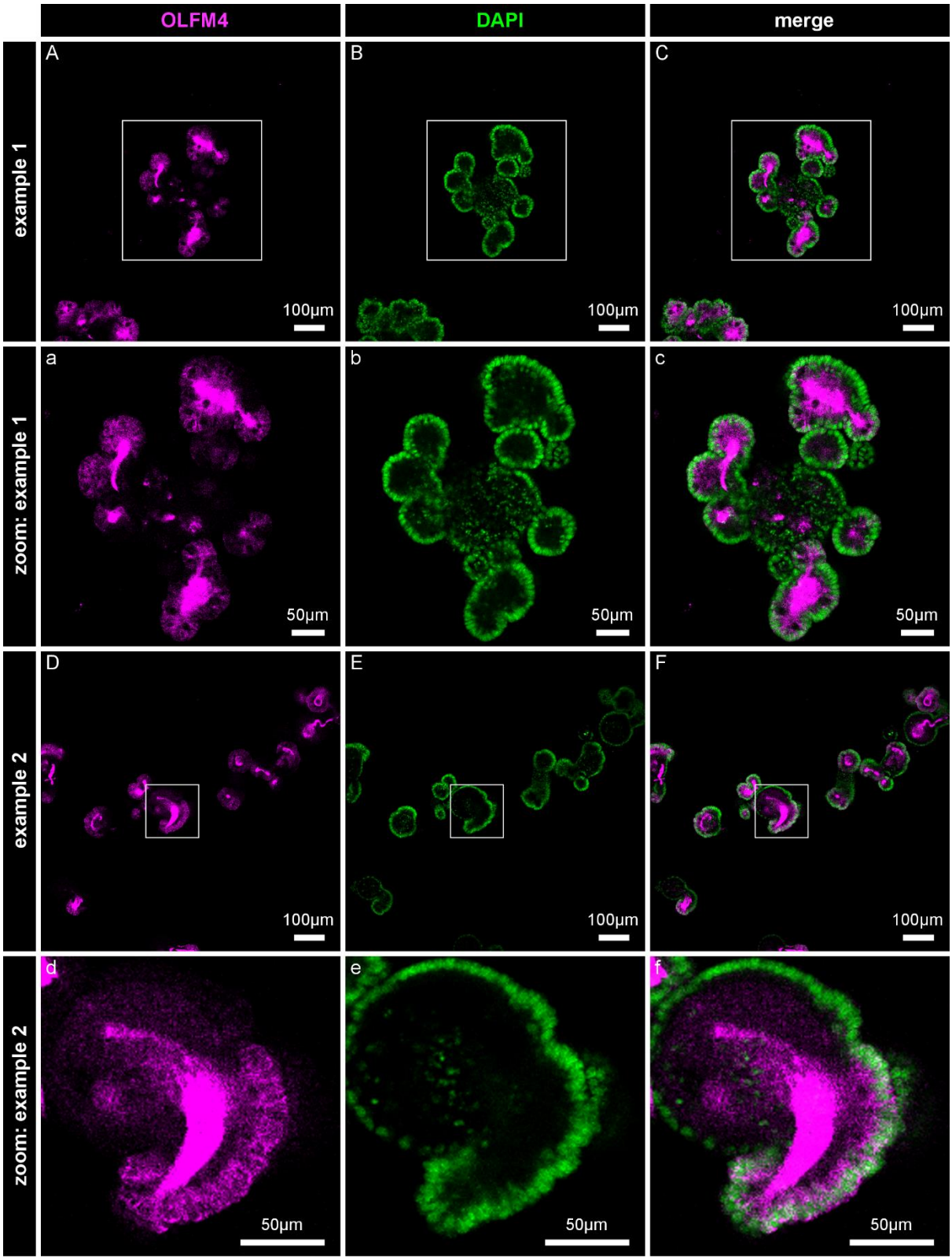

Figure 4: ***OLFM4 expression in small intestinal organoids. A-C****: example 1 of organoids stained for OLFM4,* ***a-c:*** *zoomed in version of example 1.* ***D-F****: example of 2 of organoids stained for OLFM4,* ***d-f****: zoomed in version of example 2. Confocal microscope, 20x air objective.*

2.2 Assessing the cell proliferation capacity of organoids

Having established small intestinal organoids in our laboratory, we next sought to set up a system in which to induce aneuploidy. Because of its well-established use across organisms and cell types to induce aneuploidy, we decided to treat our organoids with the MPS-1 inhibitor Reversine. Since Reversine acts at the SAC, we wanted to develop a treatment protocol that maximized the number of proliferating cells within our organoids that would be entering mitosis, and thus sensitive to Reversine during the treatment period. Although previous studies have demonstrated that cell proliferation of murine small intestinal organoids is located at the tip of the crypts (Krotenberg Garcia et al., 2021; Li et al., 2020; Sato et al., 2011), the precise quantitative extent of cell proliferation, particularly across different days of culture, remains insufficiently characterized.

We therefore attempted to quantify cell proliferation in space and time in small intestinal organoids from Day 1 post-passaging until Day 6 of culture. We used incorporation of the thymidine analog EdU (5-ethynyl-2 deoxyuridine) as a read-out for cell proliferation, which was administered to culture media either 1 hour or 2 hours before organoids fixation. We could then visualize labelling by immunofluorescence staining and confocal microscopy.

Image analysis was done by quantifying two different positions within the organoid, firstly capturing all the proliferating cells at the surface level of the organoid (***Fig. 5A-C, G-I, M-O, Fig. 6A***) and secondly quantifying proliferation at a position within the organoid (cross-section) (***Fig. 5D-E, J-L, P-R; Fig. 6B***). We could observe subtle differences between cross-section and surface quantifications (**Fig. 6A-B**). Three examples of differently aged organoids, following a 1 hour EdU pulse, are shown in panel ***A-R***. ***Figures A-F*** (example 1) depict a spheroid with no crypt formation. Cells that were actively in the cell cycle were found in every part of the organoid (***Fig. 5A, D***). Older organoids displayed budding structures where EdU-positive cells were restricted to the crypt region (**Fig. 5G-L**; example 2). Mature organoids showed proliferation only at the very tip of the bud (***Fig. 5M-R***; example 3). Across all measurement positions, the proportion of EdU-positive cells was high at Day 1 of culture, and then exhibited a statistically significant drop at Day 2. Proliferation dynamics were somewhat heterogeneous and exhibited fluctuating trends across the subsequent days. For example, in our other surface measurements, we observed that once the culture reached 3 days of age an increase in EdU incorporation was observed again, having a local maximum at Day 5 (***Fig. 6A-B***). In our cross-section measurements, we found that EdU-positive cells increase at Day 6. We performed the same experiments with a two-hour EdU-pulse instead of a one-hour pulse and observed similar dynamics: a proliferation peak at Day 1 of culture, decreasing proliferation for Day 2 and 3 and an increase from Day 4 onward (***Supplementary Fig. S1***).

In summary, we found that Day 1 post-passaging is when our culture consistently exhibits the highest proportion of proliferating cells. We therefore decided to move forward with this time point to optimise Reversine treatment.

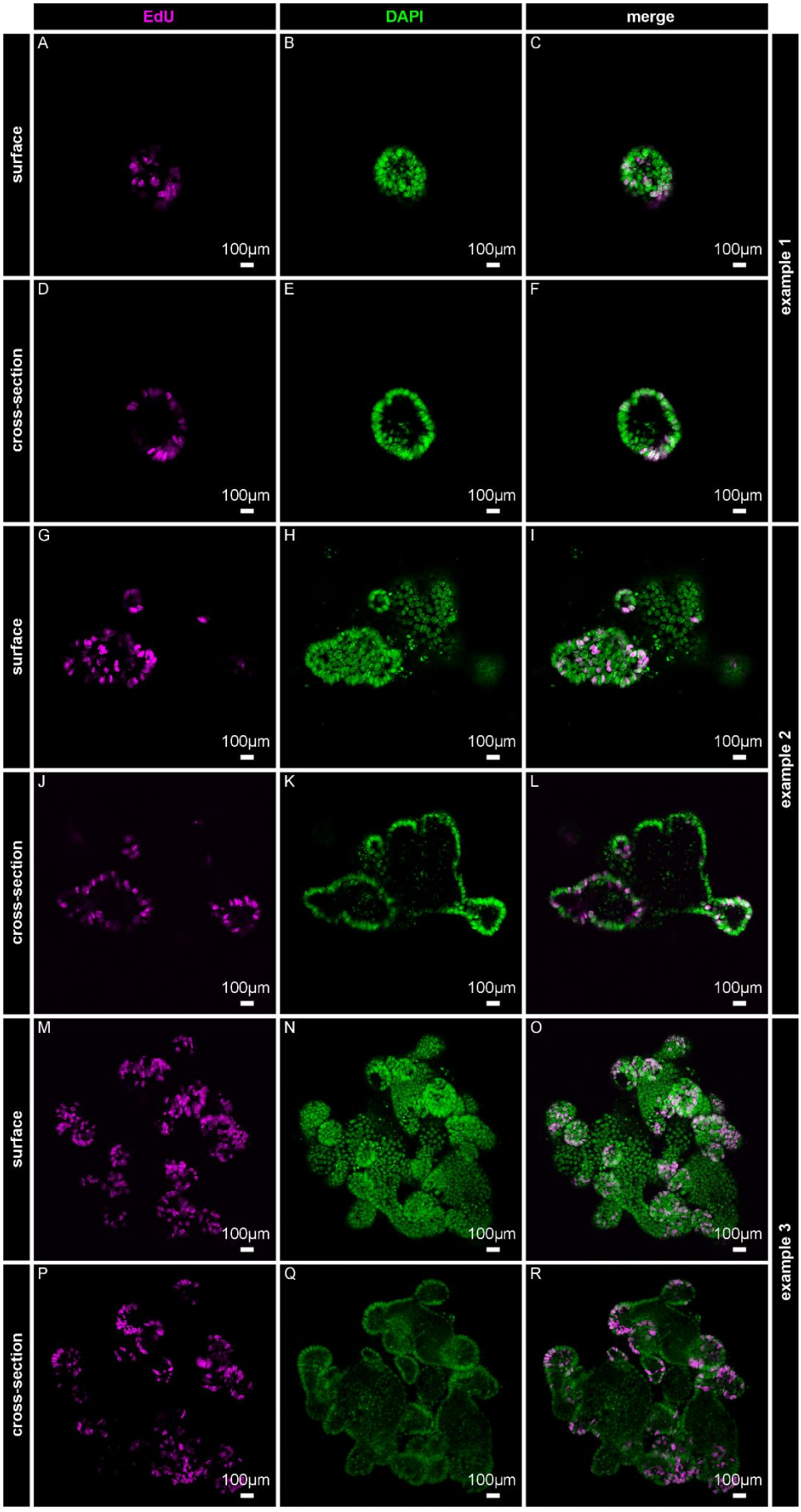
EdU
DAPI
merge
surface
cross-section
example 1
example 2
example 3
A
B
C
D
E
F
G
H
I
J
K
L
M
N
O
P
Q
R
100µm

*Figure 5: **Cell proliferation in small intestinal organoids of different ages**. **A-C, G-I, M-O**: cross-section of an organoid. **D-F, J-L, P-R:** surface of an organoid. **A-F**: 1-day old organoid. **G-L**: 4-day old organoid. **M-R**: 6-day old organoid. EdU was used as a marker of cell proliferation. Confocal images, 20x air objective.*

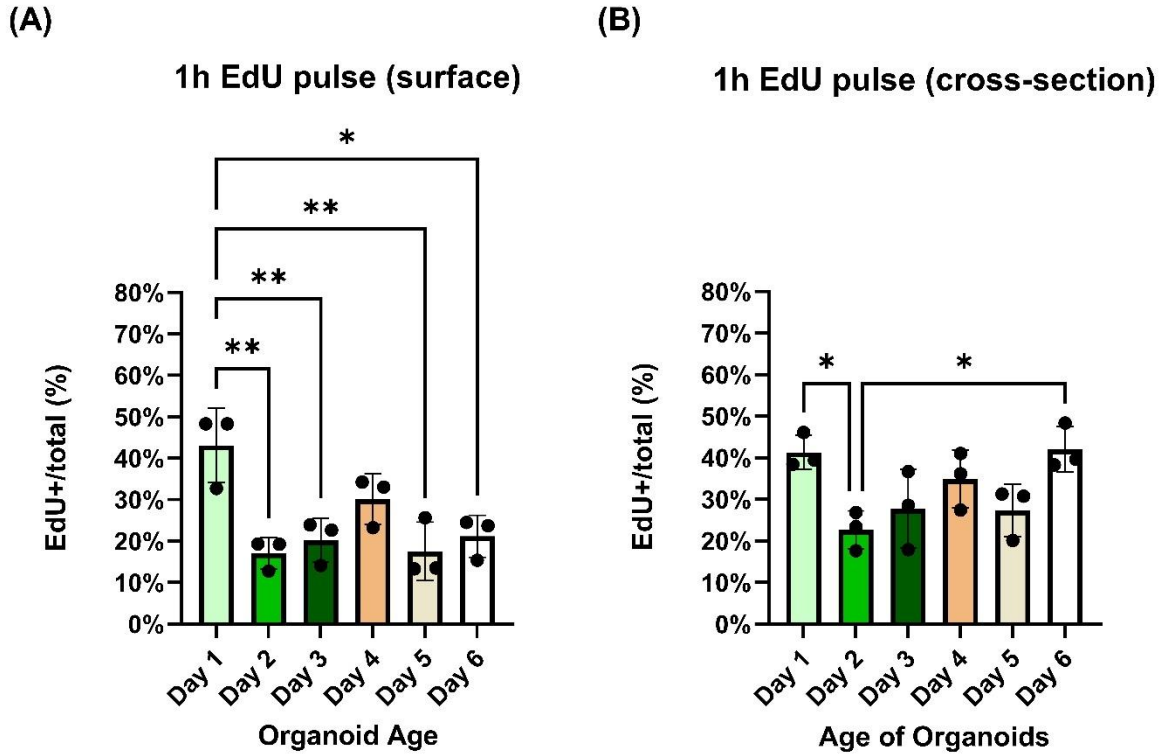

*Figure 6: **Quantification of cell proliferation in small intestinal organoids after 1h EdU pulse using immunofluorescence**. **(A)** Quantification of EdU+/total number of cells at surface level of organoids, **(B)** Quantification of EdU+/total number of cells at cross-section of organoids. Each dot represents one organoid. Statistical Analysis: One-way ANOVA, multiple comparisons: $p < 0.05$.*

2.3 Deciphering the adequate Reversine concentration

We next aimed to introduce aneuploidy in our system by treating the organoids with the MPS1 inhibitor Reversine.

First, we tested a series of Reversine concentrations to determine the optimal dosage that would induce detectable aneuploidy in organoids, without significantly compromising their viability. Taken various literature into account and performing some preliminary concentration tests, we reasoned that an effective range between 100nM and 1µM of Reversine should be tested. Subsequently, three specific concentrations within this range were selected to assess morphological stages and changes across 4-days of organoid culture. As discussed in the previous section, applying Reversine at day 1 of culture was decided upon because it displayed the highest percentage of proliferating cells (**Fig. 6A, B**) and the aim was to induce aneuploidy in as many as possible cells. Therefore, in all cases Reversine was applied according to the treatment-regime depicted in **Figure 7**; one day after passaging (Day 0 of Reversine treatment) the organoids were exposed to either 250nM, 500nM or 1µM of Reversine. Twenty four hours (24h) later a drug-washout was performed. The morphology of organoids was assessed prior to treatment, as well as 24h and 48h post Reversine administration.

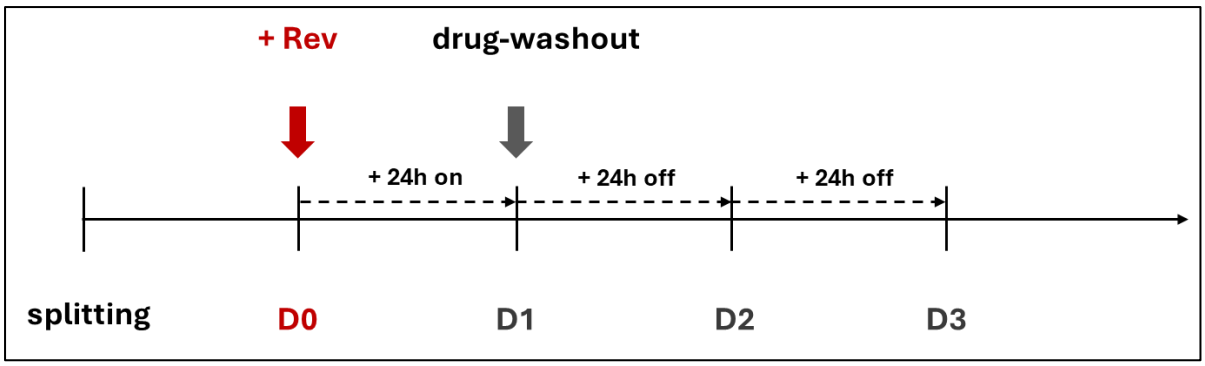

***Figure 7**: Reversine treatment-regime. D = Day, Rev = Reversine*

The morphology of the organoids was assessed at each time point, and they were classified into 5 different stages (***Fig. 8***). Stage 1 described organoids without any bud-protrusions (*spheroid stage*). Stage 2 included organoids with fewer than 3 buds (*immature stage*), whereas, organoids with three or more buds were categorized as stage 3 (*mature stage 1*). Stage 4 described organoids with a necrotic core (*mature stage 2*), and lastly stage 5 contained all organoids that stopped proliferation and underwent death irrespective of their morphological state.

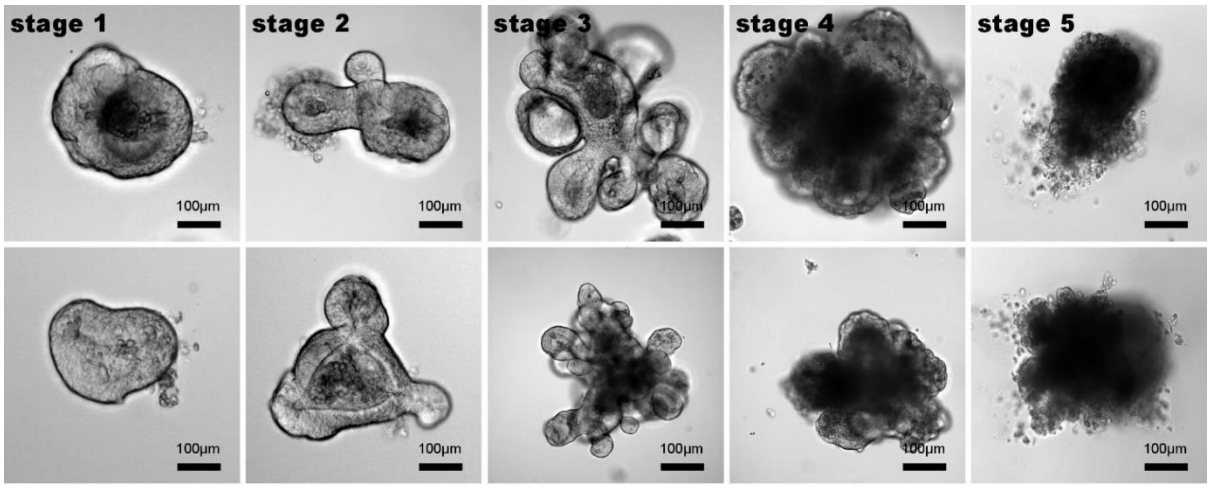

***Figure 8**: Morphological stages of small intestinal organoids. Representative images of stages 1 to 5. **Stage 1**: organoid lumen without buds (**spheroid stage**); **stage 2**: organoids with 1 or 2 buds (**immature stage**); **stage 3**: organoid with 3 or more buds (**mature stage 1**); **stage 4**: organoid with dark necrotic core (**mature stage 2**), **stage 5**: dying organoid. Brightfield microscope, 20x air objective.*

Untreated controls depicted the natural progressing of the organoid culture through the different stages. At Day 0 and Day 1 all untreated organoids classified were approximately evenly distributed across stages 1, 2 or 3; the proportion of organoids belonging to stage 3 was slightly smaller (***Fig. 9A-B***). Stages 4 and 5 were not present in the untreated organoid population on Day 0 and 1 (***Fig. 9A-B***). At Day 2 the number of organoids being at stage 1 and 2 was significantly decreased and a majority of untreated organoids were classified within stage 3 (more than 50%), but stages 4 and 5 still were not observed at this timepoint (***Fig. 9C***). At day 3, a small number of untreated organoids entered stage 4 and 5, while most of them remained classified as stage 3. Around 30% of the population at day 3 remained in stage 1 or 2 (***Fig. 9D***).

Reversine-treated organoid populations were distributed across the stages 1 to 3, with similar ratios when compared to DMSO and untreated controls at Day 1 of Reversine treatment. No major

differences between the 3 different Reversine concentrations were detected (***Fig. 9B***). 24h post-Reversine treatment organoids with necrotic cores or dying organoids appeared (stages 4 and 5) in all the Reversine-treated organoid cultures (250nM, 500nM and 1µM). The DMSO treated wells hardly showed any organoid belonging to stage 4 or 5 (***Fig. 9C***). The biggest contrast between the different Reversine concentrations was seen at Day 3 (48h post-treatment) where almost 50% of the 1µM treated cell population was undergoing cell death (stage 5). Organoids that had received 250nM or 500nM Reversine only displayed around 20% of organoids in stage 5, while maintaining 80% of the entire organoids in stages 1-4. No major difference between the treatment conditions of 250nM and 500nM could be detected. While stages 4 and 5 could also be observed in DMSO-treated controls, only 10% of the entire organoids categorized as one of those stages (***Fig. 9D***). Importantly, across all days, no major distinction between the untreated and DMSO-treated controls in their contribution to different stages could be made (***Fig. 9A-D***).

In summary, our findings showed that 24h treatment with 1µM of Reversine is too highly concentrated and leads to massive cell death. Reversine concentrations of 250nM and 500nM were better tolerated, resulting in at least 80% of the entire organoid culture still being viable and usable for downstream experiments. Ultimately, a Reversine concentration of 500nM was chosen as the working concentration.

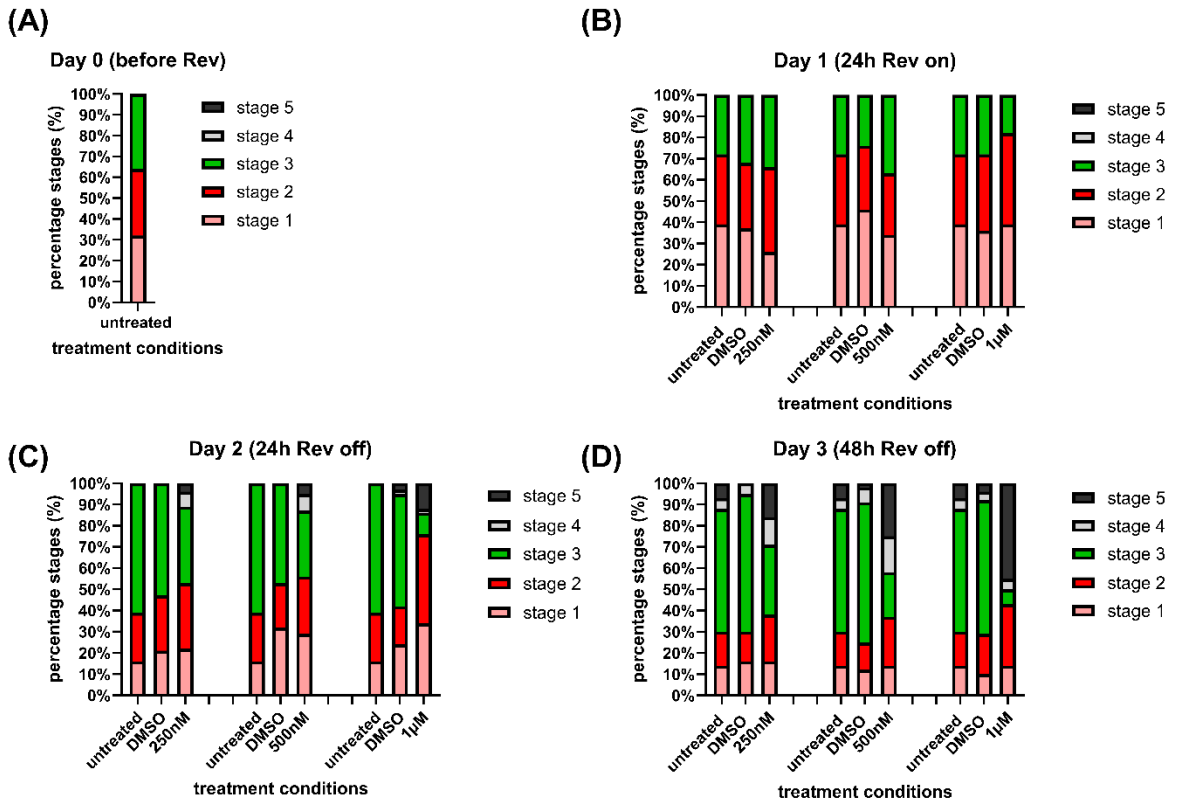

Figure 9*: Analysis of organoid developmental stages during 24h Reversine treatment across the time course of 72h. (A)* ***Day 0****: before Reversine (Rev) treatment, (B)* ***Day 1****: after 24h in Reversine, (C)* ***Day 2****: 24h after Reversine wash-out, (D)* ***Day 3****: 48h after Reversine wash-out*.

2.4. Detection of Aneuploidy in small intestinal organoids

Following Reversine treatment, we assessed our organoids for evidence of aneuploidy using confocal microscopy and immunofluorescence imaging. We managed to detect a single instance of a dividing cell that appeared to have a lagging chromosome in Reversine-treated organoids, indicating a possible mitotic defect in the affected cells. ***Figure 10B*** showcases a potential lagging chromosome seemingly "stuck" between the separated chromosome mass, compared to a normal cell division, in which chromosomes are clearly segregated at two separate poles (***Fig. 10A***). We did not observe any lagging chromosomes in control-treated cultures.

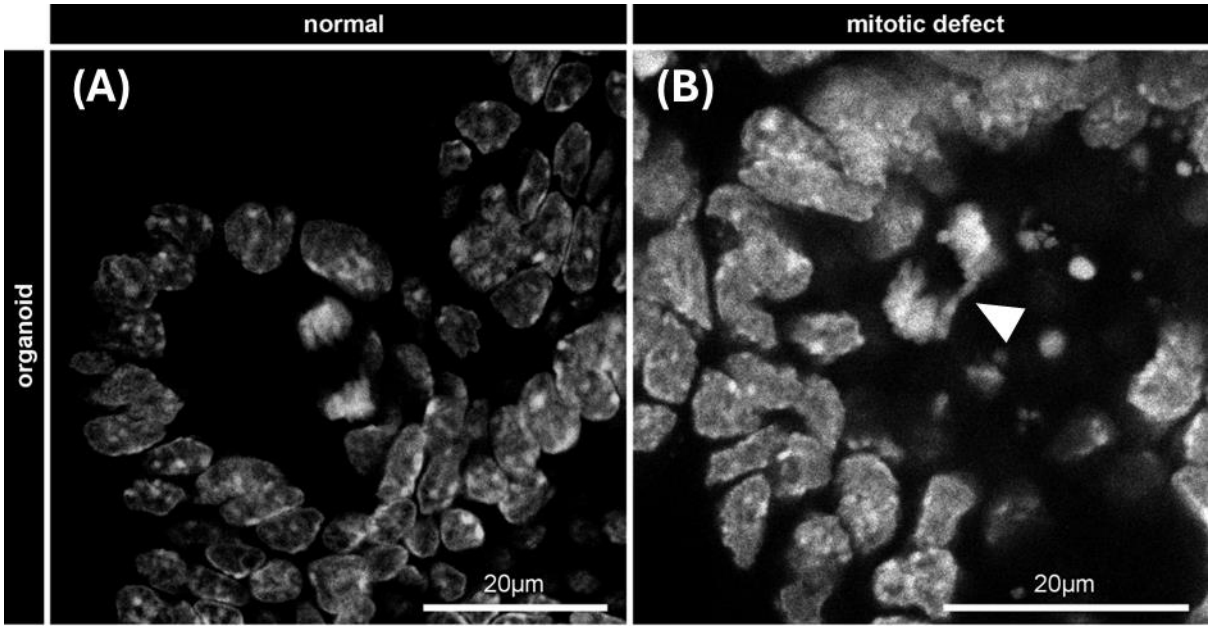

***Figure 10**: **Mitotic defects (lagging chromosome) in 3D organoids**. **(A)** normal cell division: no defects, **(B)** mitotic defect. Confocal microscope, 40x oil objective.*

2.5. Simplifying the system: from 3D to 2D – establishing and validating enteroid monolayers

Although we were heartened to discover some evidence of mitotic defects in our organoids, clear visualization and identification of such defects was very challenging in the context of the complex tissue architecture of the organoid. Exemplifying this point is the fact that we were only able to identify a single mitotic defect in the prior section. To circumvent this challenge and enable simplified identification and tracking of mitotic cells, we established a 2-dimensional enteroid monolayer system by adapting the protocol of (Ordóñez-Morán, 2020). Briefly, this system recapitulates the patterning of the three-dimensional tissue on a 2-dimensional surface thus facilitating more straight-forward imaging and characterization of cell behaviour in a single imaging plane.

To validate the enteroid monolayer system, in our laboratory, we first began by assessing several key features of the system. The cultured enteroid monolayers displayed the typical regionalization of differentiating, villi-like and proliferative crypt-like regions. The morphologically distinct crypt-zones containing multiple, densely packed nuclei were encapsulated by zones containing differentiated cells, which are less dense, and have higher heterogeneity in cell shapes (***Fig. 11a-d, e-h, Fig. 12M-P, I-J***). As expected, the cells at the very center of the crypt-like regions were positive for the intestinal stem cell marker, olfactomedin-4 (OLFM4; ***Fig. 11e-h***). They were also positive for Ki67, indicative of

proliferative activity (***Fig. 12I-L***). In contrast, the differentiated regions were OLFM4-negative (Fig. ***11a-d***) and void of any proliferation (Ki67-)(***Fig. 12M-P***).

Altogether, we are confident that we successfully established a 2D enteroid monolayer system that recapitulates the structures of the small intestine. This system can now be used for further experiments to validate the effects of Reversine, and to study tissue-level aneuploidy responses in the intestine.

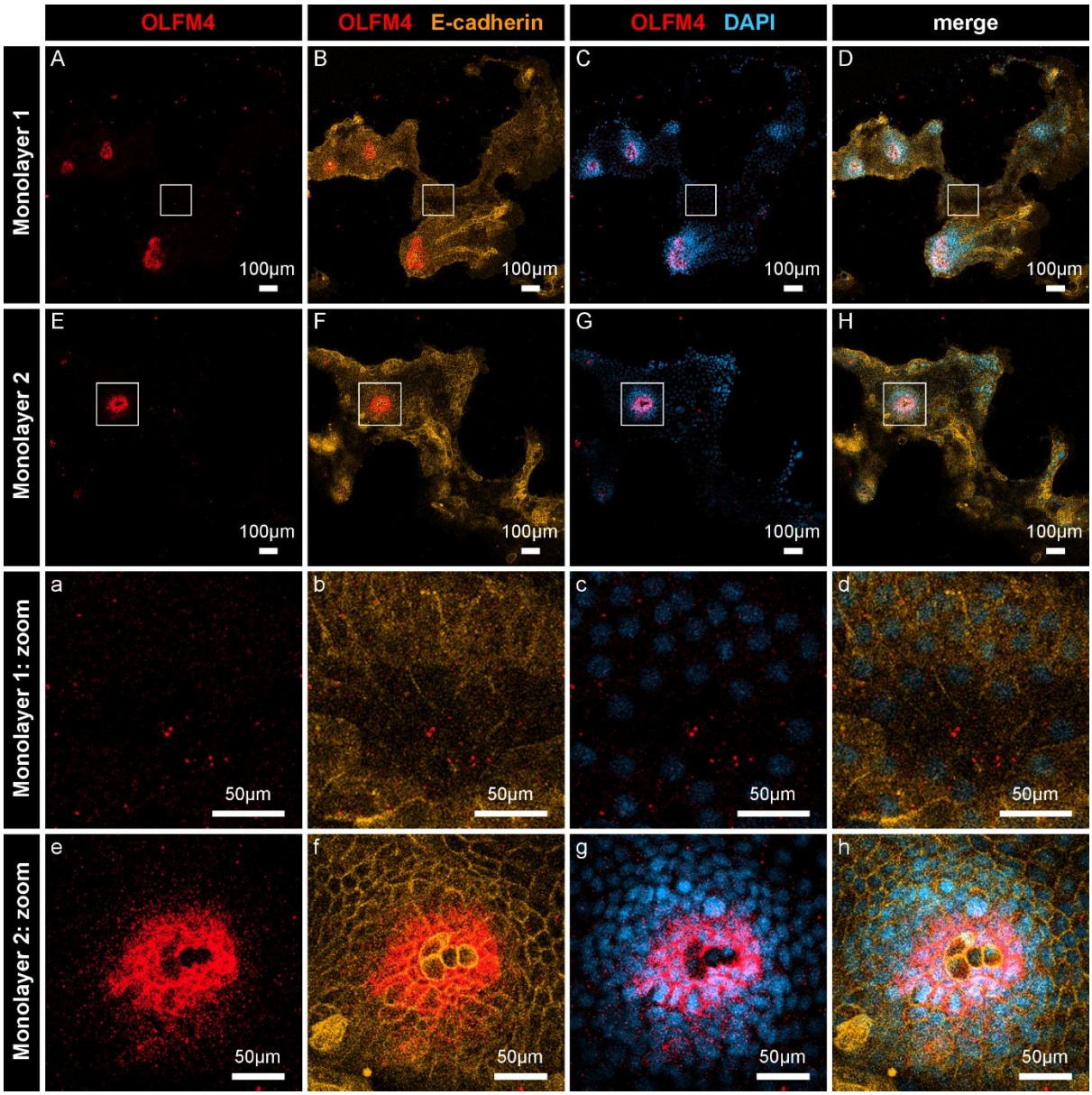

Figure 11: Characterization of 2D enteroid monolayer with the stem cell marker OLFM4*. **A-D**: example of a monolayer. **E-H**: example of a monolayer. **a-d**: zoomed-in example of a villi-like region from monolayer A-D. **e-h**: zoomed-in example of a crypt-like region from monolayer E-H. Confocal microscope, 10x air objective.*

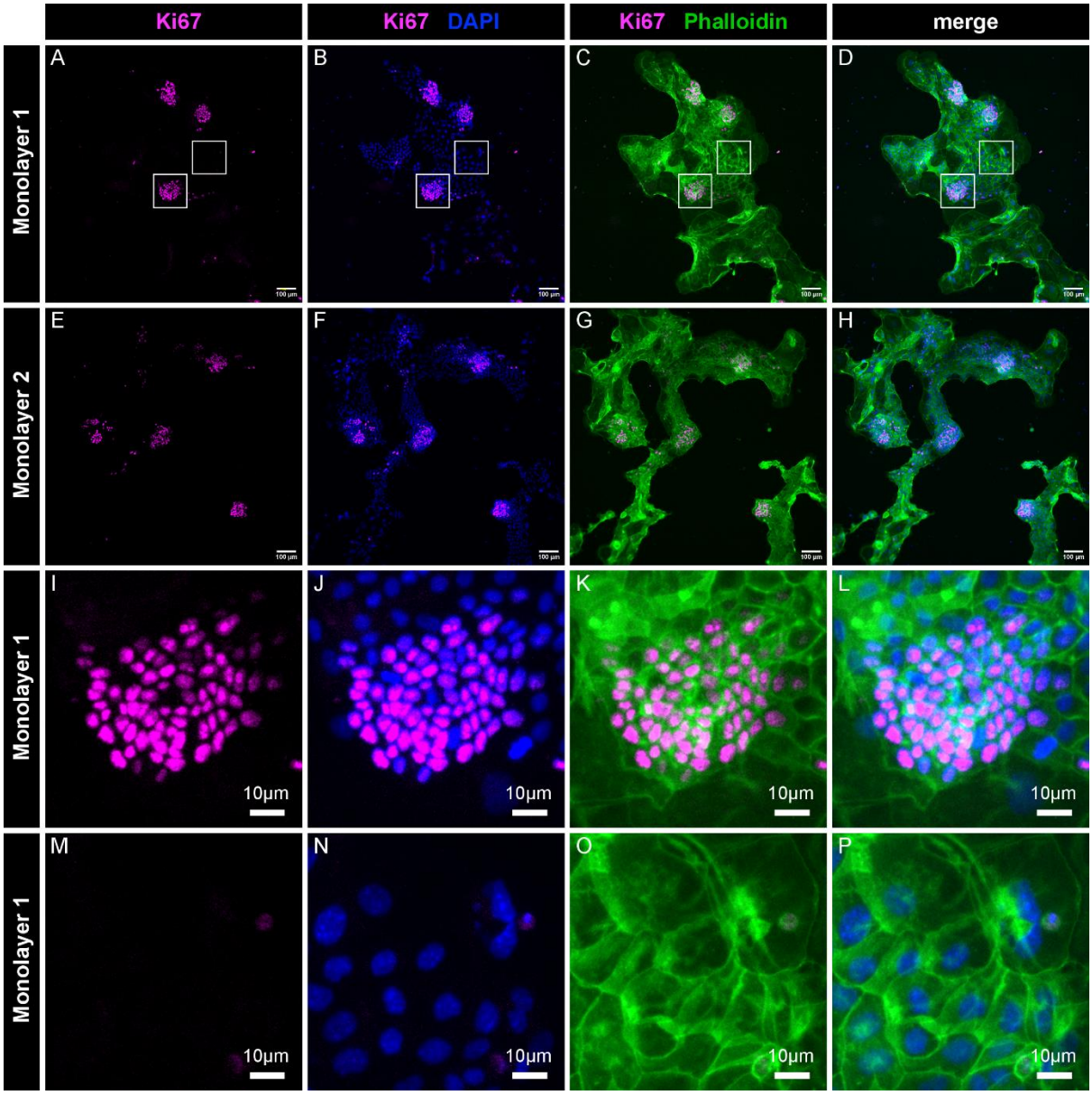

***Figure 12*: Characterization of enteroid monolayers with the proliferative marker Ki67**. **A-D**: *example of one monolayer.* **E-H:** *example of one monolayer.* **I-J**: *zoomed-in monolayer showcasing proliferative Ki67+ crypt-like cells.* **M-P**: *zoomed-in monolayer displaying differentiated Ki67- villi-like regions. Brightfield Microscope, 10x air objective*.

2.6. Detection of Aneuploidy in enteroid monolayers of the murine small intestine

We next aimed to detect mitotic defects and/or the consequences of aneuploidy in 2D enteroid monolayers. We treated our cultures with the same Reversine-treatment regimen as we established for the three-dimensional organoids (500nM Reversine for 24h) and assessed individual mitoses. In addition to looking at mitotic figures with DAPI stain, we also assessed p53, p-H2AX and cleaved caspase 3 (CC3) levels with immunofluorescence. The upregulation of p53 is implicated in response to aneuploidy in some systems (Johnson et al., 2024; Marques & Kops, 2023; Narkar et al., 2021). Similarly DNA damage, which can bet detected through accumulation of p-H2AX signal, can be a consequence of aberrant karyotypes (Johnson et al., 2024; Narkar et al., 2021). Removal of

aneuploid cells has been reported to be facilitated by apoptosis in some cases (Bolton et al., 2016; Joy et al., 2024; Singla et al., 2020). Therefore, we looked at CC3 as marker for apoptosis.

Using our 2D system, we detected a variety of abnormal mitoses (***Fig. 13A-C***). Figure A depicts a chromosome bridge, a form of physical connection (string-like structure) between the two segregated chromosome masses of sister cells. Normally at the end of anaphase the two spindle poles should contain DNA clearly separated at each pole without any physical connection, as seen in ***Figure 13B***. We also detected lagging chromosomes, another defect that can result in chromosome segregation failures during mitosis (***Figure 13B, C***).

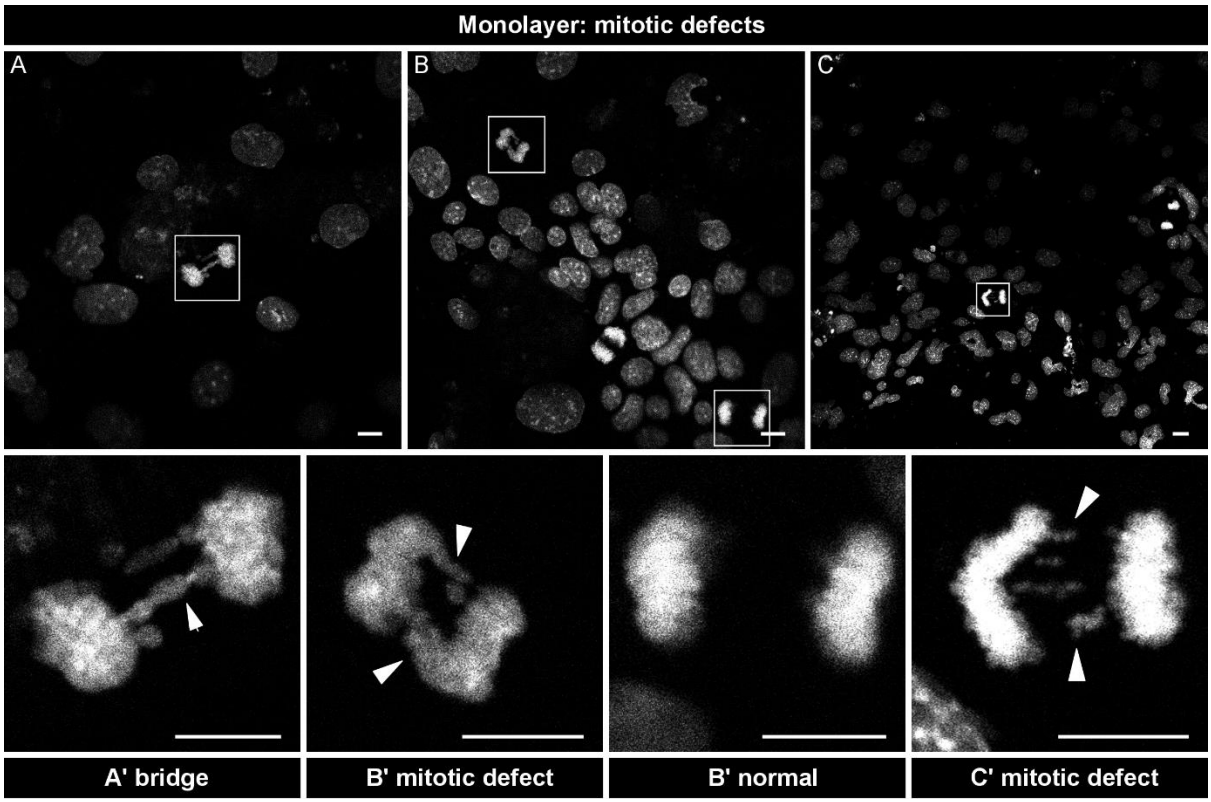

***Figure 13**: Mitotic defects in an enteroid monolayer treated with 500nM Reversine, 24h. **A, A')** mitotic defect; **B, B')** mitotic defect; **B,B')** normal mitosis: no defects; **C,C')** mitotic defect. Confocal microscope, 20x air objective, scale bar 10µm.*

Next, we quantified the mean grey intensity values of p53 in enteroid monolayers treated with Reversine or DMSO. Reversine-treated enteroid monolayers displayed a statistically significant increase in p53 (***Fig. 14A***), however the difference between the means of the two groups is small, raising some questions pertaining to biological significance (***Fig. 14B***).

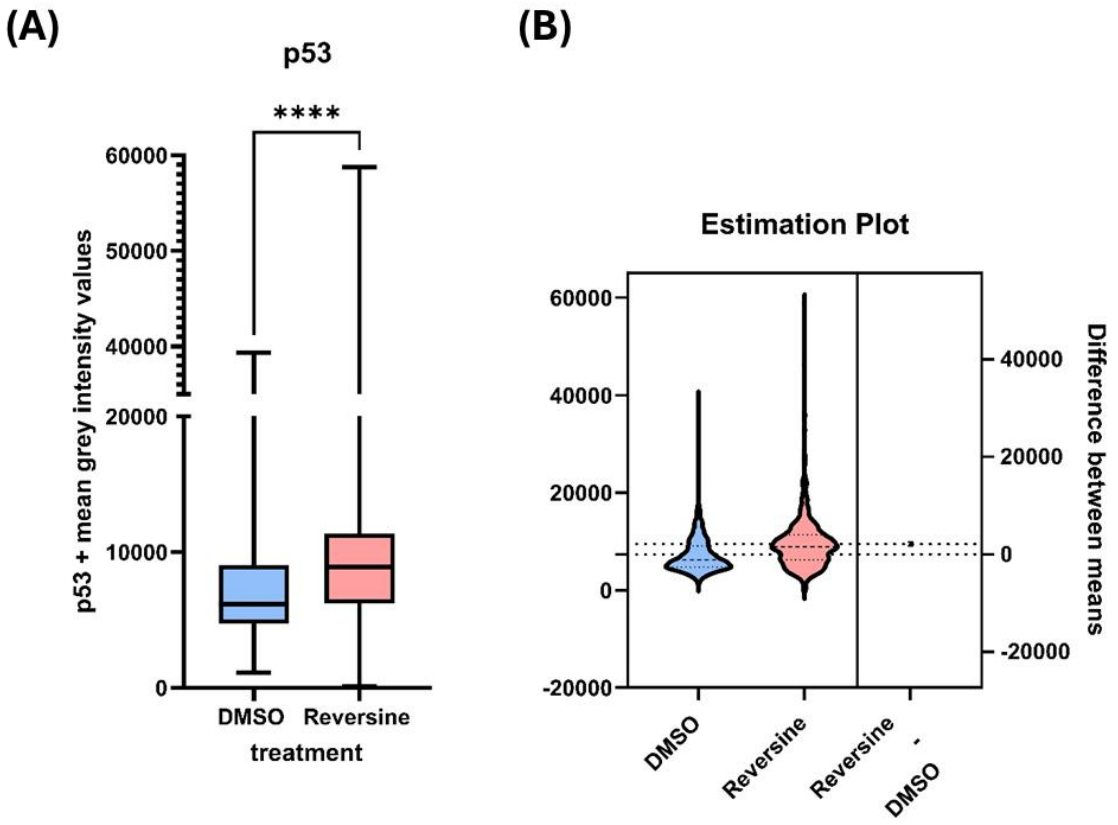

Figure 14: ***Comparison of mean grey intensity values of p53 between DMSO- (control) and Reversine-treated enteroid monolayers****. **A)** mean grey intensity levels. **B)** estimation plot. Statistical analysis: unpaired t-test with Welch's correction. $p < 0.05$. n = 4 (2 biological and 2 technical replicates per treatment).*

Differences in DNA damage between Reversine- and DMSO-treated controls were evaluated, using the DNA damage marker p-H2AX. Mean grey intensity levels from z-stacks were extracted and compared. No significant difference was detected between Reversine-treated and DMSO-treated enteroid monolayers (***Fig. 15A-B***).

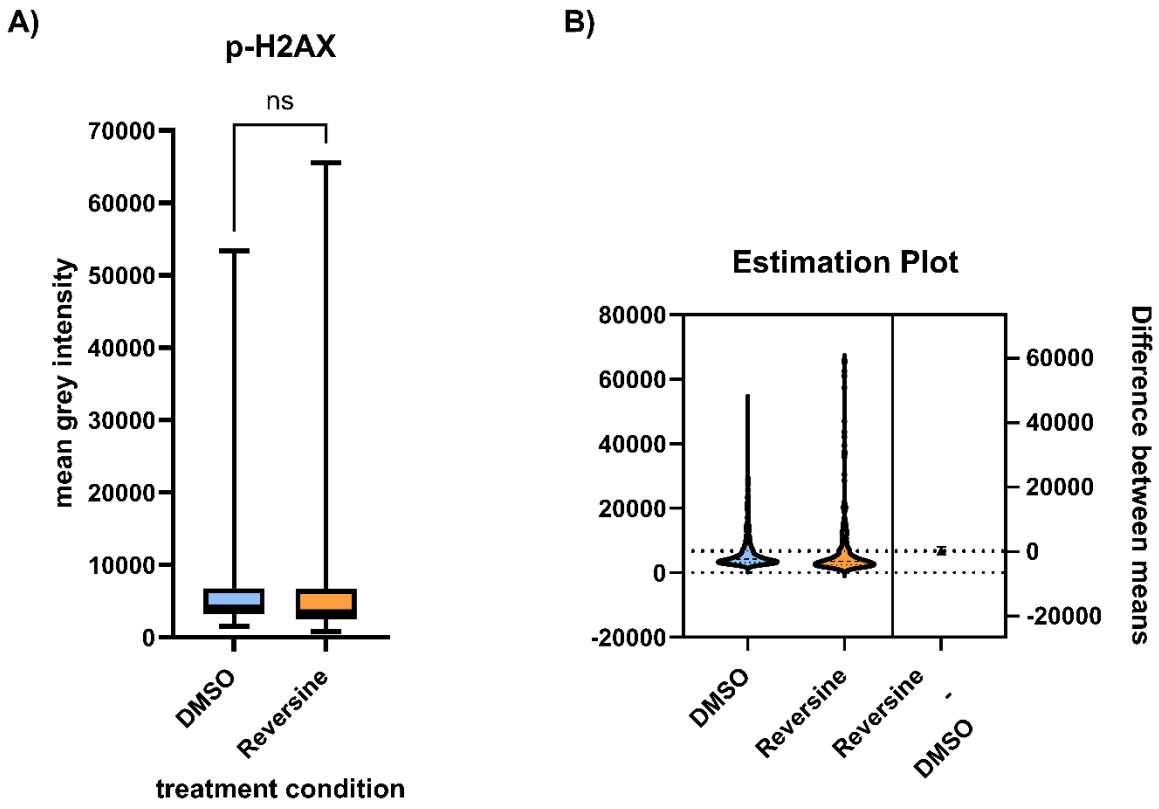

Figure 16: ***Comparison of mean grey intensity values of p-H2AX between DMSO- (control) and Reversine-treated enteroid monolayers****. **A)** mean grey intensity levels. **B)** estimation plot. Statistical analysis: unpaired t-test with Welch's correction. p < 0.05. n = 2 (2 technical replicates per treatment)*

Finally, apoptosis was assessed within the enteroid monolayer by quantifying the number of cleaved caspase-3 positive cells relative to the total cell number. Cells were untreated (baseline), treated with DMSO (control), or Reversine-treated, and images were subsequently analysed for caspase-3 activation. While untreated and DMSO-treated enteroid monolayers had similar levels of CC3 positive cells, Reversine-treated enteroid monolayers displayed increased levels, with over 9% of the cells being CC3 positive (***Fig. 16***).

Altogether these results suggest that aneuploidy causes the upregulation of p53, possibly leading to p53-mediated apoptosis of aneuploid cells, indicated by increases CC3 levels. DNA damage does not seem to be the primary inducer of p53 upregulation.

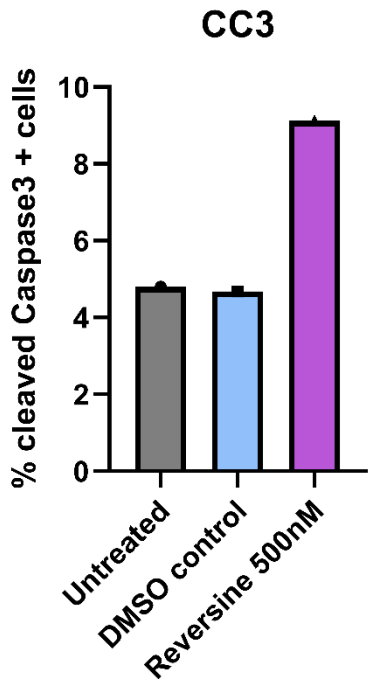

***Figure 16*: Percentage of Cleaved Caspase3 (CC3) positive cells in enteroid monolayers under different treatment conditions: untreated, DMSO control, Reversine-treated.** *N = 2 per condition (technical replicates).*

3 Discussion and Outlook

Altogether we successfully established and characterized 3D organoid and 2D enteroid monolayer cultures while contributing to more detailed characterization of the morphogenesis of crypt-derived organoids by looking at proliferation dynamics. We were able to develop a Reversine-treatment regime that induced mitotic defects in organoids and enteroid monolayers. Lastly, we made first steps in elucidating the consequences of aneuploidy induction in intestinal monolayers by looking at p53, p-H2AX and CC3 levels within the Reversine-treated enteroid monolayer.

Our work elucidates that proliferation in small intestinal organoid cultures reaches a local maximum at Day 1 of culture, however actively cycling cells can be found at each day of the culture. We demonstrated that a 24h-treatment of 500nM Reversine is tolerated by the organoids, and is sufficient for aneuploidy induction. Similarly, mitotic defects following the Reversine treatment in enteroid monolayers were observed. Further analysis of aneuploid enteroid monolayers revealed p53 and CC3 upregulation, while no increase in DNA damage (p-H2AX) was detected.

In terms of proliferation, we showed a peak at Day 1 of culture (***Fig. 6A-B***), suggesting that this timepoint is optimal to apply our aneuploidy inducing-drug Reversine, since we wanted to target cells that were actively dividing. However, due to the necrotic core of organoids and the limitations of 2D imaging, we were only able to quantify cells visible within the imaging plane of our acquired z-stacks. While this experimental approach might not fully capture the number of total cells or cycling cells, it provides preliminary insights into cell proliferation, suggesting the highest levels of cell proliferation occurring at Day 1 of culture. Since the complex 3D structure of intestinal organoids leads to a lot of light scattering when trying to acquire confocal images tissue clearing approaches might improve the resolution, allowing for more precise image analysis. With the help of tissue clearing sharper 2D images can be obtained for every plane, allowing for 3D reconstruction of the entire organoid in programs such as IMARIS. Such protocols have been successfully established and applied in intestinal organoids (Chen et al., 2013). This would allow us to gain an even deeper understanding of individual cellular events while maintaining all the spatial information.

Reversine treatment was administered after 1 day of culture, followed by 24h of drug incubation, drug washout, and a subsequent 24-h recovery period. Reversine at a concentration of 500nM was our working concentration, as it did not drastically affect viability of the organoids (***Fig. 9D***). To our surprise, proliferation increased from day 4 onwards after a decrease in proliferation at day 2 and 3 of culture (***Fig. 6A-B***). A possible explanation for the burst in proliferation could be the replenishment of fresh media, and thus new growth factors and nutrients, since media exchange was performed every 2-3 days. The presence of actively cycling cells even at day 6 of culture is reassuring, since it indicates that stem cells are maintained in the culture system and can be propagated into a new culture upon passaging. The entire Reversine dose-response assay is based on morphology changes, which are sometimes hard to detect. Even though we tried to apply a universal staging scheme, it is possible that other techniques will allow a more accurate evaluation. Another research group already established a pipeline to analyse EdU- and propodium-iodide-positive cells harvested from organoid cultures using flow cytometry (Li et al., 2020). Adapting that protocol for EdU- and propodium-iodide-stained organoids in our system has the potential for a more precise assessment of different Reversine concentrations. This way, we would be able to quantitatively determine proliferation and cell death of every cell. Often cells with highly abnormal karyotypes show defects in proliferation (Ben-David & Amon, 2020; Garribba et al., 2023; Johnson et al., 2024; Narkar et al., 2021); specifically looking at possible proliferation defects in Reversine treated cultures (such as reduced EdU incorporation), would allow to determine if aneuploidy causes

growth reduction or arrest. While analysis with flow cytometry provides a tool to quantitatively assess proliferation and cell death it leads to loss of spatial and morphological information.

The upregulation of p53 in response to aneuploidy seems to be very dependent on tissue context as well as on the degree of aneuploidy (Johnson et al., 2024; Narkar et al., 2021; Santaguida et al., 2017). Our data suggests that p53 is upregulated in response to aneuploidy (***Fig. 14A***). However, our immunofluorescence analysis was performed with a polyclonal pan-p53 antibody, leading to detection of complete p53 protein levels (including active and inactive forms) within the cell. At basal levels every cell expresses low levels of inactive p53 which will be constantly produced and degraded (high turnover). If a cell experiences stress, for instance DNA damage, p53 is stabilized, leading to increased expression levels, and activated with the help of post-translational modifications, such as phosphorylation. The active p53 will bind to DNA targets in the nucleus and lead to the transcription of specific genes necessary for DNA-repair, apoptosis, senescence or cell cycle arrest (Abuetabh et al., 2022; Wang et al., 2023). Crucial future experiments should aim to assess basal p53 protein levels in untreated cells in order to establish a baseline. Furthermore, analysing p53 expression in aneuploid cells with different techniques such as qPCR (to assess mRNA levels) as well as Western blot analysis to specifically measure phosphorylated p53 protein levels will flesh out our understanding of potential p53-mediated mechanisms at play. Of particular interest would be assessment of mRNA levels of effectors downstream pf p53 that mediate potential cellular responses to aneuploidy, including apoptosis.

While some studies in cell lines suggest p53 upregulation is a result of DNA damage associated with aneuploidy (Santaguida et al., 2017), others studies performed in colonoids do not support that claim (Johnson et al., 2024; Narkar et al., 2021). We assessed DNA damage (DNA damage marker pH2AX) in our system comparing Reversine-treated and control groups, but could not detect any significant differences (***Fig. 15A-B***). Despite our data being preliminary, it is a first step in unravelling the mechanisms of aneuploidy in the small intestine. Further experiments that can provide insights include increasing the replicate sizes for data analysis, assessing baseline levels of DNA-damage in an untreated control and quantifying DNA damage at later time points of Reversine treatment. Later time points, such as 48h after drug washout instead of the analysed 24h, might provide us with additional biological insights: maybe DNA damage is a consequence of aneuploidy, that only manifests itself after multiple cell cycles which could only be observed at later timepoints. Another important set of experiments would be assessing whether p53 upregulation is indeed triggered by aneuploidy-induced DNA damage, through blocking DNA damage repair pathways (e.g. blocking the ATM kinase involved in the DNA damage response pathway) and quantifying p53 abundance.

Having increased CC3 levels in aneuploidy induced enteroid monolayer cultures (***Fig. 16***) suggests that the small intestine potentially “senses” aneuploid cells and removes them via apoptosis. The preliminary data we show requires further validation; live imaging approaches which allow for tracking of aneuploid cells with fluorescently labelled chromatin (e.g. H2B-RFP) will help decipher if cells carrying aberrant karyotypes, are removed from organoids through apoptosis. Subsequently, we could block apoptosis using caspase inhibitors (e.g. the pan-caspase blocker Z-VAD-FMK) and measure the proportion of aneuploid cells that is retained in the culture system. If apoptosis is the mechanism by which karyotypically aberrant cells are cleared from the tissue, we would expect to see an accumulation of aneuploid cells in Reversine-treated cultures.

Recent studies demonstrated that the cellular response to aneuploidy depends on the overall level of aneuploidy that is present. Generally aberrant karyotypes can be classified as simple or complex, referring to either higher (complex) or lower numbers (simple) of changed chromosomes. It was shown that simple aneuploid cells continue to proliferate, do not upregulate p53 and no cell cycle

arrest can be observed. Conversely, cells carrying more severe aberrant karyotypes, halt their proliferation, upregulate p53 and undergo cell cycle arrest. This was demonstrated in monolayer cultures as well as 3D organoid cultures (Garribba et al., 2023; Johnson et al., 2024; Santaguida et al., 2017). It is therefore important to mention that all our experiments were performed with high concentrations of Reversine to induce complex chromosomal changes. However, generating chronic/simple levels of aneuploidy by applying lower concentrations of Reversine, over a prolonged time window, might be an intriguing route to take to determine if simple aberrant karyotypes are better tolerated in the intestinal tissue. Pre-liminary data showed that organoid cultures treated with lower Reversine concentrations displayed similar morphology to their untreated counterparts and were able to reestablish organoid cultures post-passaging (***Fig. S2A-F***). Ultimately it remains to be determined if aneuploid cells were simply eliminated in those organoid cultures or if the aneuploid cells could get propagated to the next culture. Ongoing experiments in the lab will aim to clarify which of the two possibilities explains our observations.

Despite some visible aneuploid effects, that were induced with Reversine, it is still a drug that upon wash-out will no longer block the spindle checkpoint kinase. Therefore, having a genetic tool to permanently interfere with chromosomal segregation would be extremely helpful. Overexpression of polo like kinase 4 (PLK4) is an alternative strategy to induce aneuploidy that has been previously utilized in the small intestine (Levine et al., 2017). Additionally the overexpression construct can be designed to carry a fluorescent protein, allowing us to label and track individual aneuploid cells. PLK4 is needed for centriole duplication (Habedanck et al., 2005) and its overexpression leads to supernumerary centrosomes. Consequently, pseudo-bipolar spindles assemble, causing abnormal cell divisions, ultimately resulting in aneuploidy. Studies showed that overexpression of PLK4 protein in mammalian epidermis led to p53-dependent apoptotic removal of cells with abnormal karyotypes within the tissue. Transplantation experiments in flies demonstrated that increased centrosome number causes tumor formation (Levine et al., 2017; Serçin et al., 2016). Assessment of different tissues after PLK4-overexpression showcases that the increase of aneuploid cells and enhanced proliferation varies broadly between tissues, highlighting once more the importance of tissue context (Levine et al., 2017). Nevertheless, PLK4 overexpression could provide a genetic alternative to stably induce chromosome mis-segregation in small intestinal organoids. We are currently in the process of generating organoids carrying the PLK4-overexpression construct with the hope of gaining more crucial insights in the world of aneuploidy in the intestine.

It is not clear whether the apoptotic response we observe in Reversine-treated organoids is a cell autonomous response to aneuploidy, or rather a cell non-autonomous response that depends on the presence of healthy euploid neighbours as it has been postulated in other systems. To test this possibility we aim to generate pure populations of wild-type organoid-cells and aneuploid cells that can be mixed within an organoid, subsequently assessing the faith of aneuploid cells especially those in contact with neighbouring wild-type cells. The establishment of mixed organoids has already been shown (Garcia et al., 2021). Such mixed population experiments will allow us to more directly assess how the local neighbourhood of an aneuploid cell influences its survival.

Having looked at aneuploidy in the small intestine it would be of great interest to perform the same and even additional experiments in the colon to gain more insights into potential similarities and differences between the two tissues regarding aneuploidy. We have recently set up a colonoid culture system in our laboratory by using a modified version of an already established protocol by O'Rourke and colleagues (O'Rourke et al., 2016). By performing similar experiments in the colon, we could probe the response of the large intestine to aneuploidy induction when compared to the small intestine. A study already demonstrated that abnormal karyotypes can be induced in the colon using

Reversine (Johnson et al., 2024), suggesting that the small intestine is perhaps more efficient in removing aneuploid cells and less tolerant towards them.

Finally, most aneuploidies in humans are embryonically lethal, but some karyotypic aberrations like trisomy 21 are sometimes compatible with life (Santaguida et al., 2017). By generating induced pluripotent stem cells (iPSCs) from individuals with abnormal karyotypes, human intestinal organoids exhibiting chronic levels of aneuploidy could be obtained. Protocols that generate intestinal organoids from iPSCs are already established and available (Durczak et al., 2024; Mithal et al., 2020). By using patient-derived organoids that stably harbour aneuploid cells that are evidently compatible with life, one could set up mixed organoids with euploid counterparts to see how aneuploid cells would get removed from the organoid tissue by euploid cells and if so, what mechanism would be at play.

Taken together, these results suggest that p53-mediated apoptosis could be at play in the small intestine to drive removal of aneuploid cells. The direct causes of p53 upregulation must be determined since we could not correlate it to increased DNA damage. Further follow-up experiments are needed to unravel possible mechanisms underlying survival versus elimination of cells carrying aberrant karyotypes.

4 Material and Methods

4.1 Methods

4.1.1 Primary 3D organoid culture from isolated small intestinal crypts

For establishing small intestinal organoids from primary intestinal tissue, we followed the protocol of Sato and Clevers (2012). Briefly, the mice were sacrificed according to ethical guidelines, the small intestine was isolated and flushed with cold PBS. Afterwards it was cut open longitudinally and villi were removed by gently scrapping with a coverslip, followed by cutting the intestine into smaller pieces. Then more PBS-washes were performed after which the intestinal pieces were incubated in cold 2mM EDTA for 30min, at 4°C. Multiple fractions were generated by vigorously pipetting up and down to isolate the crypts from the intestinal pieces. Each fraction was checked under the microscope and the fraction containing the most crypts was filtered through a 70µm filter, followed by centrifugation and 3 more washing steps. 250 crypts per 24-well were plated in a 50µl Matrigel droplet. The organoids were incubated at 37°C, 5% CO2. After 4 days organoids should start to form.

4.1.2 Enteroid Monolayer generated from 3D small intestinal organoids

For establishing the enteroid monolayer the protocol from Ordóñez-Morán (2020) was followed. Briefly, already established 3D organoids were detached, dissociated and enzymatically digested using the TrypLE enzyme. Once a single cell suspension was obtained 50 000 or 100 000 cells were plated per well in a 96-well imaging plate. For culturing, plating media containing Chiron and Y-27632 was used. After 18-24 hours the plating media was replaced by small intestinal complete media only, which was subsequently replaced every two days until the enteroid monolayer reached optimal confluency.

4.1.3 Maintenance of 3D organoid culture

The organoids were split every 5-7 days or once they displayed a necrotic core. For culturing small intestinal complete media was used which was exchanged every 2-3 days.

Organoid splitting was performed by adding 1 mL of ice-cold basal media to each well to detach the organoids from the Matrigel matrix. The resulting organoid suspension was transferred to a tube, and the well was washed with an additional 1 mL of basal media. The suspension was then subjected to mechanical disruption by pipetting up and down with a P1000 pipette (20x), followed by a P200 pipette (10x) to shear and fragment the organoids into smaller aggregates. Subsequently, the organoids were washed with 10 mL of ice-cold basal media followed by centrifugation (200xg, 5min, 4°C). This washing process was repeated two more times before the organoid pellet was resuspended in the according volume of Matrigel, which was then seeded into a 24-well plate.

4.1.4 Immunofluorescence staining of whole mount 3D organoids

After removing the media and washing the organoids twice with PBS, they were fixed for 20min in 4% PFA at room temperature. The organoids were then washed off the well using PBS and transferred into a flacon tube. Three more wash-steps with PBS were performed, followed by incubating the samples in 0.3% Triton in PBS at RT on a shaker. Blocking was performed with 0.3% Blocking buffer solution for an 1h at room temperature. Lastly the organoids were incubated in the primary antibody solution overnight at 4°C on a shaker. On the next day, five more washing steps in 0.3% PBS-T were performed, before incubating for at least 1h in secondary antibody solution. The

organoids were washed three more times in PBS and subsequently mounted on glass slides. The slides were left overnight to dry.

4.1.5 Immunofluorescence staining of enteroid monolayer

After the enteroid monolayer had reached optimal confluency, it was fixed using 4% Paraformaldehyde diluted in PBS for 15-20min at room temperature. Afterwards the wells were rinsed two times with PBS before they were permeabilized using 0.3% PBS-T (0,3% Triton X-100 in PBS). Blocking was performed for 1 hour at room temperature (RT) using 0.3% blocking buffer. After blocking the monolayer was incubated in primary antibody solution over night at 4°C (antibodies were diluted in blocking buffer). The enteroid monolayer was washed 3 more times with 0.3% PBS-T for 5min each at RT before incubating with the secondary antibody for at least 1h at RT. DAPI was diluted in blocking buffer of 1:10 000 or 1:5000 (corresponding to a final concentration of 0.5µg/ml or 1µg/ml) and the samples were incubated for 10-15minutes at RT. Finally, the wells were washed 2 times with PBS-T and the final wash was performed with PBS.

4.1.6 Reversine treatment

4.1.6.1. 3D organoids

Organoids were treated with 500nM of Reversine 24h after they were split. The treatment was carried out for 24h if not otherwise indicated. After the completed drug-treatment, the organoids were washed with PBS and cultured in complete intestinal media for another 24h before they were harvested or utilized in subsequent experiments.

4.1.6.2. Enteroid Monolayer

Reversine treatment (Reversine concentration: 500nM) was carried out once the enteroid monolayer reached optimal confluency. This was usually achieved after two or three days in culture. Enteroid monolayer cultures were treated for 24h with Reversine, followed by wash-out and 24h culture without Reversine, after which the enteroid monolayer was fixed for further analysis.

4.1.7 EdU incorporation and immunofluorescence

The Invitrogen Click-iT EdU Cell proliferation Kit for Imaging (Alexa Flour 647) was used to detect cell proliferation in organoids. Organoids were incubated with 10µM EdU for either 1h or 2h after which they were fixed with 4% PFA for 20min at room temperature (RT).

For immunofluorescence the protocol provided by Invitrogen was adapted: After fixation the organoids were washed 3x with PBS for 15 minutes. Permeabilization was performed using 0.3% PBS-T for 30min at RT. Blocking was executed for 1h at RT (0.3% blocking buffer) followed by primary antibody incubation over night at 4°C. Three washing steps with 0.3% PBS-T (15min each) were performed, followed by washing in 1x 3% BSA (Bovine serum albumin) dissolved in PBS. Click-iT reaction cocktail was prepared following the companies' instructions, and the samples were incubated for 45min, at RT in the dark. The organoids were washed 1x with 3% BSA and 3x with 0.3% PBS-T before they were left in secondary antibody solution for 2h at RT. DAPI staining was conducted using a concentration of 0.5µg/ml or 1µg/ml of DAPI in blocking buffer for 10-15 minutes at RT. Two final washes in 0.3% PBS-T and one final wash in PBS was performed.

All antibodies were diluted in 0.3% blocking buffer. All washing steps were performed at room temperature.

4.1.8. Microscopy

All confocal images were acquired using the Zeiss LSM 980 Confocal microscope, with either the 10x, 20x or the 40x oil objective.

Brightfield images were recorded by using the inverted fluorescence Zeiss Widefield Microscope Axio Observer Z1, with either 10x or 20x magnification.

Image processing was performed using the ImageJ (1.54f) software from Wayne Rasband and contributors.

4.1.9 Image analysis EdU quantification with ImageJ

The MAX intensity projection of every acquired z-stack of chosen slices was used and converted into an 8-bit image. Thresholding for the EdU channel was performed (Default option, adjusted as needed). After thresholding the EdU and DAPI channel were overlaid, and counting was performed. Per organoids the cells at the surface of the enteroid were quantified, called surface quantification. Cross-section quantifications were done by choosing planes within the z-stack in which the broadest part of the organoid was depicted.

4.1.10 Media composition

4.1.10.1 Small intestinal basal media

Advanced DMEM/F12 media was supplemented with HEPES (final concentration: 10mM), GlutaMAX (final concentration 2mM) and Penicillin-Streptomycin (final concentration 100U/mL, 100µg/mL).

4.1.10.2 Small intestinal organoid complete media

The basal media was complemented with B27 (final concentration 1x), N2 (final concentration 1X), N-Acetylcysteine (final concentration: 50ng/mL), EGF mouse (final concentration: 50ng/mL), Noggin (final concentration: 50ng/mL), R-spondin-1 (final concentration: 50ng/mL or 1x).

For the complete media either purified R-spondin-1 growth factor or R-spondin-1-conditioned media was utilized. No detectable difference in organoid growth was observed between the two formulations."

4.1.10.3 Enteroid Monolayer - Plating media

For the plating media CHIR-99021 (final concentration: 3µM) and ROCK-inhibitors (final concentration: 10µM) were added to small intestinal organoids complete media.

4.1.11 Crypt Isolation buffer

EDTA was dissolved in DPBS (without Magnesium and Calcium) to a final concentration of 2mM. The buffer was sterile filtered.

4.1.12 Fixing solution

4% Paraformaldehyde was used for fixing, we diluted 16% of Paraformaldehyde in 1x PBS.

4.1.13 Blocking buffer

The blocking buffer was prepared in 1x PBS containing 1% BSA, 0.3% Triton Tx-100, 2.5% fish gelatine and 0.4% normal donkey serum.

4.2 Material

4.2.1 Antibody list

Name	Protein	Host	Dilution immunofluorescence	Company
Cleaved Caspase-3 (Asp175) Antibody #9661	Cleaved caspase 3	Rabbit	1:300	Cell Signaling Technology Catalog # 9661
CD324 (E-Cadherin) Monoclonal Antibody (DECMA-1), eBioscience™	E-cadherin	Rat	1:200	Invitrogen Catalog # 14-3249-82
Phospho-Histone H2A.X (Ser139) (20E3) Rabbit mAb #9718	γ-H2AX	Rabbit	1:500	Cell Signaling Technology Catalog #9718
Olfm4 (D6Y5A) XP® Rabbit mAb #39141	OLFM4	Rabbit	1:200	Cell Signaling Technology Catalog #39141
p53 Protein (CM5)	p53	Rabbit	1:500	Leica Biosystems NCL-L-p53-CM5p
ChromoTek rat anti RFP Monoclonal antibody (5F8)	RFP	Rat	1:300	Proteintech Cat No. 5f8

4.2.2 Material used

- Fisher Scientific Corning™ Matrigel™ GFR Basement Membrane Matrix; Product Code 11523550
- Fisher Scientific Corning™ Sterile Cell Strainers, Product Code 15370801
- Fisher Scientific Invitrogen™ DAPI and Hoechst Nucleic Acid Stains; Product Code 11530306
- Fisher Scientific Invitrogen™ Click-iT™ EdU Cell Proliferation Kit for Imaging, Alexa Fluor™ 647 dye; Product Code 10063724
- Gibco™ Advanced DMEM/F12; Catalog number 12634010
- Gibco™ B-27™ Supplement (50X), serum free; Catalog number 17504044
- Gibco™ GlutaMAX™ Supplement; Catalog number 35050061
- Gibco Mouse EGF Recombinant Protein; Catalog # PMG8045
- Gibco Mouse Noggin Recombinant Protein, PeproTech®; Catalog # 250-38-250UG
- Gibco™ N-2 Supplement (100X); Catalog number 17502048
- Gibco™ Penicillin-Streptomycin (10,000 U/mL); Catalog number 15140122
- Gibco™ TrypLE™ Express Enzyme (1X), no phenol red; Catalog number 12604039
- Merck ROCK Inhibitor (Y-27632); Product number SCM075
- Sigma Aldrich Bovine Serum Albumin; 10735078001
- Sigma-Aldrich Donkey Serum, 100 ml; S30-100ML
- Sigma-Aldrich Gelatin from cold water fish skin; G7765-1L
- Sigma-Aldrich N-Acetyl-L-Cysteine; A9165-5G

- Tebubio CHIR-99021; Catalog Number 10-1279
- Thermo Scientific™ 96 Well Black/Clear Bottom Plate, TC Surface; Catalog number 165305
- Thermo Scientific Chemicals Paraformaldehyde, 16% w/v aq. soln., methanol free; Catalog number 043368.9M

5 References

Abuetabh, Y., Wu, H. H., Chai, C., Al Yousef, H., Persad, S., Sergi, C. M., & Leng, R. (2022). DNA damage response revisited: The p53 family and its regulators provide endless cancer therapy opportunities. *Experimental & Molecular Medicine*, *54*(10), 1658–1669. https://doi.org/10.1038/s12276-022-00863-4

Ağagündüz, D., Cocozza, E., Cemali, Ö., Bayazıt, A. D., Nanì, M. F., Cerqua, I., Morgillo, F., Saygılı, S. K., Berni Canani, R., Amero, P., & Capasso, R. (2023). Understanding the role of the gut microbiome in gastrointestinal cancer: A review. *Frontiers in Pharmacology*, *14*, 1130562. https://doi.org/10.3389/fphar.2023.1130562

Almeqdadi, M., Mana, M. D., Roper, J., & Yilmaz, Ö. H. (2019). Gut organoids: Mini-tissues in culture to study intestinal physiology and disease. *American Journal of Physiology - Cell Physiology*, *317*(3), C405–C419. https://doi.org/10.1152/ajpcell.00300.2017

Altay, G., Larrañaga, E., Tosi, S., Barriga, F. M., Batlle, E., Fernández-Majada, V., & Martínez, E. (2019). Self-organized intestinal epithelial monolayers in crypt and villus-like domains show effective barrier function. *Scientific Reports*, *9*(1), 10140. https://doi.org/10.1038/s41598-019-46497-x

Azzouz, L. L., & Sharma, S. (2025). Physiology, Large Intestine. In *StatPearls*. StatPearls Publishing. http://www.ncbi.nlm.nih.gov/books/NBK507857/

Baker, D. J., Chen, J., & van Deursen, J. M. (2005). The mitotic checkpoint in cancer and aging: What have mice taught us? *Current Opinion in Cell Biology*, *17*(6), 583–589. https://doi.org/10.1016/j.ceb.2005.09.011

Barker, N., van Es, J. H., Kuipers, J., Kujala, P., van den Born, M., Cozijnsen, M., Haegebarth, A., Korving, J., Begthel, H., Peters, P. J., & Clevers, H. (2007). Identification of stem cells in small intestine and colon by marker gene Lgr5. *Nature*, *449*(7165), 1003–1007. https://doi.org/10.1038/nature06196

Barnum, K. J., & O'Connell, M. J. (2014). Cell Cycle Regulation by Checkpoints. *Methods in Molecular Biology (Clifton, N.J.)*, *1170*, 29–40. https://doi.org/10.1007/978-1-4939-0888-2_2

Barsouk, A., Rawla, P., Barsouk, A., & Thandra, K. C. (2019). Epidemiology of Cancers of the Small Intestine: Trends, Risk Factors, and Prevention. *Medical Sciences*, *7*(3), 46. https://doi.org/10.3390/medsci7030046

Ben-David, U., & Amon, A. (2020). Context is everything: Aneuploidy in cancer. *Nature Reviews Genetics*, *21*(1), 44–62. https://doi.org/10.1038/s41576-019-0171-x

Bolton, H., Graham, S. J. L., Van der Aa, N., Kumar, P., Theunis, K., Fernandez Gallardo, E., Voet, T., & Zernicka-Goetz, M. (2016). Mouse model of chromosome mosaicism reveals lineage-specific depletion of aneuploid cells and normal developmental potential. *Nature Communications*, *7*(1), 11165. https://doi.org/10.1038/ncomms11165

Brás, R., Monteiro, A., Sunkel, C. E., & Resende, L. P. (2021). Aneuploidy facilitates dysplastic and tumorigenic phenotypes in the Drosophila gut. *Biology Open*, *10*(11), bio058623. https://doi.org/10.1242/bio.058623

Capdevila, C., Miller, J., Cheng, L., Kornberg, A., George, J. J., Lee, H., Botella, T., Moon, C. S., Murray, J. W., Lam, S., Calderon, R. I., Malagola, E., Whelan, G., Lin, C.-S., Han, A., Wang, T. C., Sims, P. A., & Yan, K. S. (2024). Time-resolved fate mapping identifies the intestinal upper crypt zone as an origin of Lgr5+ crypt base columnar cells. *Cell*, *187*(12), 3039-3055.e14. https://doi.org/10.1016/j.cell.2024.05.001

Chen, Y., Tsai, Y.-H., Liu, Y.-A., Lee, S.-H., Tseng, S.-H., & Tang, S.-C. (2013). Application of Three-Dimensional Imaging to the Intestinal Crypt Organoids and Biopsied Intestinal Tissues. *The Scientific World Journal*, *2013*, 624342. https://doi.org/10.1155/2013/624342

Cimini, D., Howell, B., Maddox, P., Khodjakov, A., Degrassi, F., & Salmon, E. D. (2001). Merotelic Kinetochore Orientation Is a Major Mechanism of Aneuploidy in Mitotic Mammalian Tissue Cells. *The Journal of Cell Biology*, *153*(3), 517. https://doi.org/10.1083/jcb.153.3.517

Clevers, H. (2013). The Intestinal Crypt, A Prototype Stem Cell Compartment. *Cell*, *154*(2), 274–284. https://doi.org/10.1016/j.cell.2013.07.004

Corrò, C., Novellasdemunt, L., & Li, V. S. W. (2020). A brief history of organoids. *American Journal of Physiology - Cell Physiology*, *319*(1), C151–C165. https://doi.org/10.1152/ajpcell.00120.2020

Durczak, P. M., Fair, K. L., Jinks, N., Oca&#241, S. C., a, Zu&#241, C. B. S., iga, & Hannan, N. R. F. (2024). Generation of hiPSC-Derived Intestinal Organoids for Developmental and Disease Modelling Applications. *JoVE (Journal of Visualized Experiments)*, *205*, e61199. https://doi.org/10.3791/61199

Flier, L. G. van der, Haegebarth, A., Stange, D. E., Wetering, M. van de, & Clevers, H. (2009). OLFM4 Is a Robust Marker for Stem Cells in Human Intestine and Marks a Subset of Colorectal Cancer Cells. *Gastroenterology*, *137*(1), 15–17. https://doi.org/10.1053/j.gastro.2009.05.035

Garcia, A. K., Fumagalli, A., Le, H. Q., Jackstadt, R., Lannagan, T. R. M., Sansom, O. J., Rheenen, J. van, & Suijkerbuijk, S. J. E. (2021). Active elimination of intestinal cells drives oncogenic growth in organoids. *Cell Reports*, *36*(1). https://doi.org/10.1016/j.celrep.2021.109307

Garribba, L., De Feudis, G., Martis, V., Galli, M., Dumont, M., Eliezer, Y., Wardenaar, R., Ippolito, M. R., Iyer, D. R., Tijhuis, A. E., Spierings, D. C. J., Schubert, M., Taglietti, S., Soriani, C., Gemble, S., Basto, R., Rhind, N., Foijer, F., Ben-David, U., … Santaguida, S. (2023). Short-term molecular consequences of chromosome mis-segregation for genome stability. *Nature Communications*, *14*(1), 1353. https://doi.org/10.1038/s41467-023-37095-7

Garvey, D. R., Chhabra, G., Ndiaye, M. A., & Ahmad, N. (2021). Role of Polo-Like Kinase 4 (PLK4) in Epithelial Cancers and Recent Progress in its Small Molecule Targeting for Cancer Management. *Molecular Cancer Therapeutics*, *20*(4), 632–640. https://doi.org/10.1158/1535-7163.MCT-20-0741

Gehart, H., & Clevers, H. (2019). Tales from the crypt: New insights into intestinal stem cells. *Nature Reviews Gastroenterology & Hepatology*, *16*(1), 19–34. https://doi.org/10.1038/s41575-018-0081-y

Guillot, C., & Lecuit, T. (2013). Mechanics of Epithelial Tissue Homeostasis and Morphogenesis. *Science*, *340*(6137), 1185–1189. https://doi.org/10.1126/science.1235249

Habedanck, R., Stierhof, Y.-D., Wilkinson, C. J., & Nigg, E. A. (2005). The Polo kinase Plk4 functions in centriole duplication. *Nature Cell Biology*, *7*(11), 1140–1146. https://doi.org/10.1038/ncb1320

He, Q., Au, B., Kulkarni, M., Shen, Y., Lim, K. J., Maimaiti, J., Wong, C. K., Luijten, M. N. H., Chong, H. C., Lim, E. H., Rancati, G., Sinha, I., Fu, Z., Wang, X., Connolly, J. E., & Crasta, K. C. (2018). Chromosomal instability-induced senescence potentiates cell non-autonomous tumourigenic effects. *Oncogenesis*, *7*(8), 1–18. https://doi.org/10.1038/s41389-018-0072-4

Hoevenaar, W. H. M., Janssen, A., Quirindongo, A. I., Ma, H., Klaasen, S. J., Teixeira, A., van Gerwen, B., Lansu, N., Morsink, F. H. M., Offerhaus, G. J. A., Medema, R. H., Kops, G. J. P. L., & Jelluma, N. (2020). Degree and site of chromosomal instability define its oncogenic potential. *Nature Communications*, *11*(1), 1501. https://doi.org/10.1038/s41467-020-15279-9

Holland, A. J., & Cleveland, D. W. (2012). Losing balance: The origin and impact of aneuploidy in cancer. *EMBO Reports*, *13*(6), 501–514. https://doi.org/10.1038/embor.2012.55

Ji, Z., Chuen, J., Kiparaki, M., & Baker, N. (2021). Cell competition removes segmental aneuploid cells from Drosophila imaginal disc-derived tissues based on ribosomal protein gene dose. *eLife*, *10*, e61172. https://doi.org/10.7554/eLife.61172

Johnson, B. A., Liu, A. Z., Bi, T., Dong, Y., Li, T., Zhou, D., Narkar, A., Wu, Y., Sun, S. X., Larman, T. C., Zhu, J., & Li, R. (2024). Simple aneuploidy evades p53 surveillance and promotes niche factor-independent growth in human intestinal organoids. *Molecular Biology of the Cell*, *35*(8), br15. https://doi.org/10.1091/mbc.E24-04-0166

Joy, J., Fusari, E., & Milán, M. (2024). Aneuploidy-induced cellular behaviors: Insights from Drosophila. *Developmental Cell*, *59*(3), 295–307. https://doi.org/10.1016/j.devcel.2023.12.009

Keku, T. O., Dulal, S., Deveaux, A., Jovov, B., & Han, X. (2015). The gastrointestinal microbiota and colorectal cancer. *American Journal of Physiology - Gastrointestinal and Liver Physiology*, *308*(5), G351–G363. https://doi.org/10.1152/ajpgi.00360.2012

Knouse, K. A., Wu, J., Whittaker, C. A., & Amon, A. (2014). Single cell sequencing reveals low levels of aneuploidy across mammalian tissues. *Proceedings of the National Academy of Sciences*, *111*(37), 13409–13414. https://doi.org/10.1073/pnas.1415287111

Krotenberg Garcia, A., Fumagalli, A., Le, H. Q., Jackstadt, R., Lannagan, T. R. M., Sansom, O. J., van Rheenen, J., & Suijkerbuijk, S. J. E. (2021). Active elimination of intestinal cells drives oncogenic growth in organoids. *Cell Reports*, *36*(1), 109307. https://doi.org/10.1016/j.celrep.2021.109307

Lara-Gonzalez, P., Pines, J., & Desai, A. (2021). Spindle assembly checkpoint activation and silencing at kinetochores. *Seminars in Cell & Developmental Biology*, *117*, 86–98. https://doi.org/10.1016/j.semcdb.2021.06.009

Levine, M. S., Bakker, B., Boeckx, B., Moyett, J., Lu, J., Vitre, B., Spierings, D. C., Lansdorp, P. M., Cleveland, D. W., Lambrechts, D., Foijer, F., & Holland, A. J. (2017). Centrosome amplification is sufficient to promote spontaneous tumorigenesis in mammals. *Developmental Cell*, *40*(3), 313-322.e5. https://doi.org/10.1016/j.devcel.2016.12.022

Li, H.-S., Xu, S.-F., Sheng, J.-Y., Jiang, Z.-H., Wang, J., Ding, N., Wang, T., Odenwald, M. A., Turner, J. R., He, W.-Q., Xu, H., & Zha, J.-M. (2020). Quantification of Proliferative and Dead Cells in Enteroids. *Journal of Visualized Experiments : JoVE*, *155*, 10.3791/60501. https://doi.org/10.3791/60501

Lukow, D. A., Sausville, E. L., Suri, P., Chunduri, N. K., Wieland, A., Leu, J., Smith, J. C., Girish, V., Kumar, A. A., Kendall, J., Wang, Z., Storchova, Z., & Sheltzer, J. M. (2021). Chromosomal instability accelerates the evolution of resistance to anti-cancer therapies. *Developmental Cell*, *56*(17), 2427-2439.e4. https://doi.org/10.1016/j.devcel.2021.07.009

Marques, J. F., & Kops, G. J. P. L. (2023). Permission to pass: On the role of p53 as a gatekeeper for aneuploidy. *Chromosome Research*, *31*(4), 31. https://doi.org/10.1007/s10577-023-09741-9

McAinsh, A. D., & Kops, G. J. P. L. (2023). Principles and dynamics of spindle assembly checkpoint signalling. *Nature Reviews Molecular Cell Biology*, *24*(8), 543–559. https://doi.org/10.1038/s41580-023-00593-z

Mithal, A., Capilla, A., Heinze, D., Berical, A., Villacorta-Martin, C., Vedaie, M., Jacob, A., Abo, K., Szymaniak, A., Peasley, M., Stuffer, A., Mahoney, J., Kotton, D. N., Hawkins, F., & Mostoslavsky, G. (2020). Generation of mesenchyme free intestinal organoids from human induced pluripotent stem cells. *Nature Communications*, *11*(1), 215. https://doi.org/10.1038/s41467-019-13916-6

Narkar, A., Johnson, B. A., Bharne, P., Zhu, J., Padmanaban, V., Biswas, D., Fraser, A., Iglesias, P. A., Ewald, A. J., & Li, R. (2021). On the role of p53 in the cellular response to aneuploidy. *Cell Reports*, *34*(12), 108892. https://doi.org/10.1016/j.celrep.2021.108892

Ordóñez-Morán, P. (Ed.). (2020). *Intestinal Stem Cells: Methods and Protocols* (Vol. 2171). Springer US. https://doi.org/10.1007/978-1-0716-0747-3

O'Rourke, K. P., Ackerman, S., Dow, L. E., & Lowe, S. W. (2016). Isolation, Culture, and Maintenance of Mouse Intestinal Stem Cells. *Bio-Protocol*, *6*(4), e1733.

Rao, C. V., Yang, Y.-M., Swamy, M. V., Liu, T., Fang, Y., Mahmood, R., Jhanwar-Uniyal, M., & Dai, W. (2005). Colonic tumorigenesis in BubR1+/–ApcMin/+ compound mutant mice is linked to premature separation of sister chromatids and enhanced genomic instability. *Proceedings of the National Academy of Sciences*, *102*(12), 4365–4370. https://doi.org/10.1073/pnas.0407822102

Rao, J. N., & Wang, J.-Y. (2010a). Intestinal Architecture and Development. In *Regulation of Gastrointestinal Mucosal Growth*. Morgan & Claypool Life Sciences. https://www.ncbi.nlm.nih.gov/books/NBK54098/

Rao, J. N., & Wang, J.-Y. (2010b). Intestinal Architecture and Development. In *Regulation of Gastrointestinal Mucosal Growth*. Morgan & Claypool Life Sciences. https://www.ncbi.nlm.nih.gov/books/NBK54098/

Sansregret, L., & Swanton, C. (2017). The Role of Aneuploidy in Cancer Evolution. *Cold Spring Harbor Perspectives in Medicine*, *7*(1), a028373. https://doi.org/10.1101/cshperspect.a028373

Santaguida, S., & Amon, A. (2015). Short- and long-term effects of chromosome mis-segregation and aneuploidy. *Nature Reviews Molecular Cell Biology*, *16*(8), 473–485. https://doi.org/10.1038/nrm4025

Santaguida, S., Richardson, A., Iyer, D. R., M'Saad, O., Zasadil, L., Knouse, K. A., Wong, Y. L., Rhind, N., Desai, A., & Amon, A. (2017). Chromosome mis-segregation generates cell cycle-arrested cells with complex karyotypes that are eliminated by the immune system. *Developmental Cell*, *41*(6), 638-651.e5. https://doi.org/10.1016/j.devcel.2017.05.022

Sasaki, N., Sachs, N., Wiebrands, K., Ellenbroek, S. I. J., Fumagalli, A., Lyubimova, A., Begthel, H., van den Born, M., van Es, J. H., Karthaus, W. R., Li, V. S. W., López-Iglesias, C., Peters, P. J., van Rheenen, J., van Oudenaarden, A., & Clevers, H. (2016). Reg4+ deep crypt secretory cells function as epithelial niche for Lgr5+ stem cells in colon. *Proceedings of the National Academy of Sciences of the United States of America*, *113*(37), E5399–E5407. https://doi.org/10.1073/pnas.1607327113

Sato, T., & Clevers, H. (2012). Primary Mouse Small Intestinal Epithelial Cell Cultures. In S. H. Randell & M. L. Fulcher (Eds.), *Epithelial Cell Culture Protocols* (Vol. 945, pp. 319–328). Humana Press. https://doi.org/10.1007/978-1-62703-125-7_19

Sato, T., Stange, D. E., Ferrante, M., Vries, R. G. J., Es, J. H. van, Brink, S. van den, Houdt, W. J. van, Pronk, A., Gorp, J. van, Siersema, P. D., & Clevers, H. (2011). Long-term Expansion of Epithelial Organoids From Human Colon, Adenoma, Adenocarcinoma, and Barrett's Epithelium. *Gastroenterology*, *141*(5), 1762–1772. https://doi.org/10.1053/j.gastro.2011.07.050

Sato, T., Vries, R. G., Snippert, H. J., van de Wetering, M., Barker, N., Stange, D. E., van Es, J. H., Abo, A., Kujala, P., Peters, P. J., & Clevers, H. (2009). Single Lgr5 stem cells build crypt-villus structures in vitro without a mesenchymal niche. *Nature*, *459*(7244), 262–265. https://doi.org/10.1038/nature07935

Serçin, Ö., Larsimont, J.-C., Karambelas, A. E., Marthiens, V., Moers, V., Boeckx, B., Le Mercier, M., Lambrechts, D., Basto, R., & Blanpain, C. (2016). Transient PLK4 overexpression accelerates tumorigenesis in p53-deficient epidermis. *Nature Cell Biology*, *18*(1), 100–110. https://doi.org/10.1038/ncb3270

Singla, S., Iwamoto-Stohl, L. K., Zhu, M., & Zernicka-Goetz, M. (2020). Autophagy-mediated apoptosis eliminates aneuploid cells in a mouse model of chromosome mosaicism. *Nature Communications*, *11*(1), 2958. https://doi.org/10.1038/s41467-020-16796-3

Siri, S. O., Martino, J., & Gottifredi, V. (2021). Structural Chromosome Instability: Types, Origins, Consequences, and Therapeutic Opportunities. *Cancers*, *13*(12), 3056. https://doi.org/10.3390/cancers13123056

Širvinskas, D., Omrani, O., Lu, J., Rasa, M., Krepelova, A., Adam, L., Kaeppel, S., Sommer, F., & Neri, F. (2022). Single-cell atlas of the aging mouse colon. *iScience*, *25*(5). https://doi.org/10.1016/j.isci.2022.104202

Sotillo, R., Hernando, E., Díaz-Rodríguez, E., Teruya-Feldstein, J., Cordón-Cardo, C., Lowe, S. W., & Benezra, R. (2007). Mad2 Overexpression Promotes Aneuploidy and Tumorigenesis in Mice. *Cancer Cell*, *11*(1), 9–23. https://doi.org/10.1016/j.ccr.2006.10.019

Thorne, C. A., Chen, I. W., Sanman, L. E., Cobb, M. H., Wu, L. F., & Altschuler, S. J. (2018). Enteroid monolayers reveal an autonomous WNT and BMP circuit controlling intestinal epithelial growth and organization. *Developmental Cell*, *44*(5), 624-633.e4. https://doi.org/10.1016/j.devcel.2018.01.024

Wang, H., Guo, M., Wei, H., & Chen, Y. (2023). Targeting p53 pathways: Mechanisms, structures and advances in therapy. *Signal Transduction and Targeted Therapy*, *8*(1), 1–35. https://doi.org/10.1038/s41392-023-01347-1

6 Supplementary

Quantification of cell proliferation in small intestinal organoids using EdU (2h pulse)

Cell proliferation was quantified using EdU incorporation as a read out. The EdU-pulse was performed for 2h. Organoids were stained by immunofluorescence and imaged. Those acquired z-stacks were used to conduct our quantifications. For every organoid the surface and a z-plane within the organoid (cross-section) were assessed. No difference in the trend between surface and cross-section measurements could be observed (S1, A-B). Proliferation peaked at Day 1 of culture and decreased at Day 2 and 3 (S1, A-B). More cycling cells could be observed at Day 4 and 5 when compared to the previous two days. The lowest levels of proliferation were detected at day 6 of culture (S1, A-B). While in the cross-section analysis the differences between individual days were significant (S1, B) we could not detect and significance at the surface level quantification (S1, A).

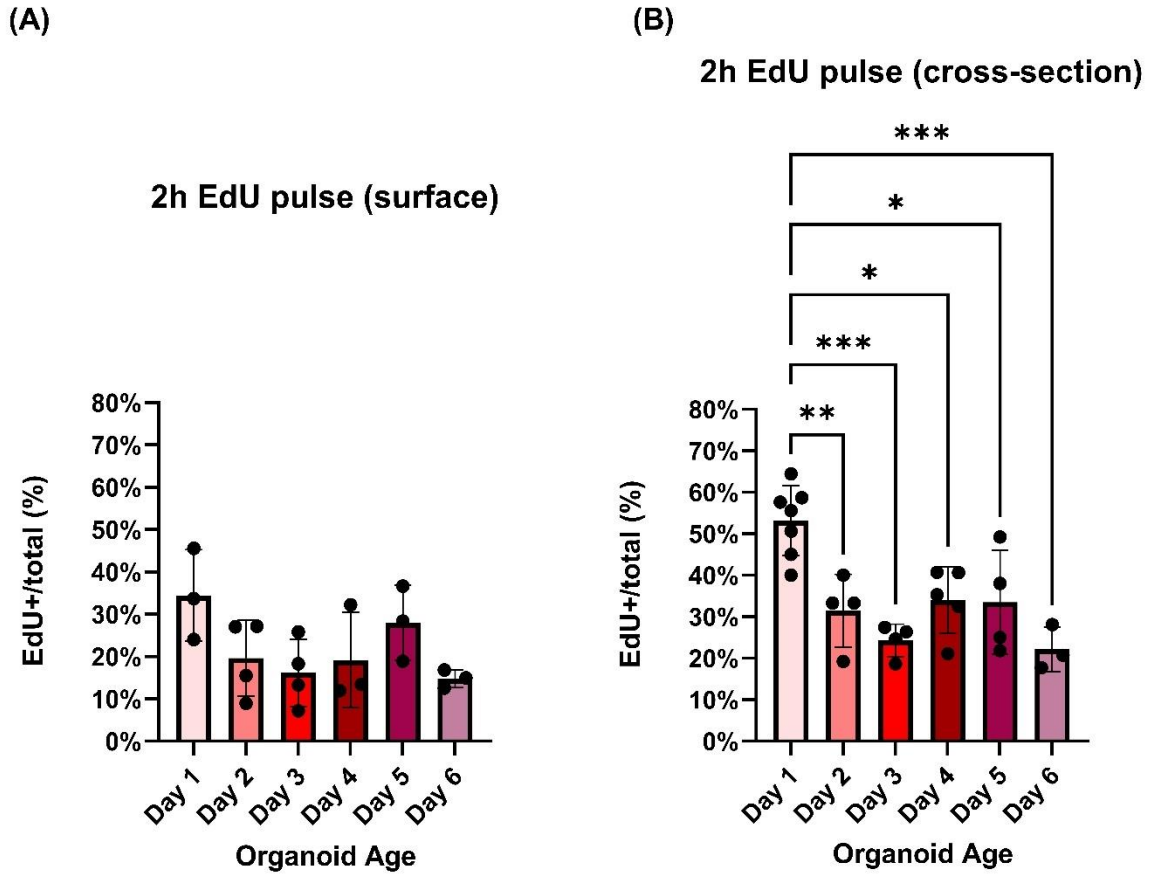

Supplementary Figure S1: *Quantification of cell proliferation in small intestinal organoids using via EdU incorporation (2h EdU pulse) using immunofluorescence. (A) Quantification at surface level of organoids, (B) Quantification at cross-section of organoids. Statistical Analysis: One-way ANOVA, multiple comparisons: alpha = 0.05.*

Reversine treated and passaged organoids (chronic aneuploidy)

We administered to the organoid culture a lower concentration of Reversine (125nM) instead of our standard concentration of 500nM one day post-splitting. The organoids stayed in Reversine for 3

days. We assed their morphology as criteria for tolerating the treatment. After 3 days of drug-media, some organoids displayed some cell death at surface level (Fig. S2A) when compared to the DMSO-treated control (Fig. S2B). After passaging the organoid culture regained their mature morphology without major cells death. No difference between the DMSO control and the treatment group could be observed 48h after splitting (Fig. S2F-G), although some cell death was visible in the treated organoids 1 day after splitting (Fig. S2C-D).

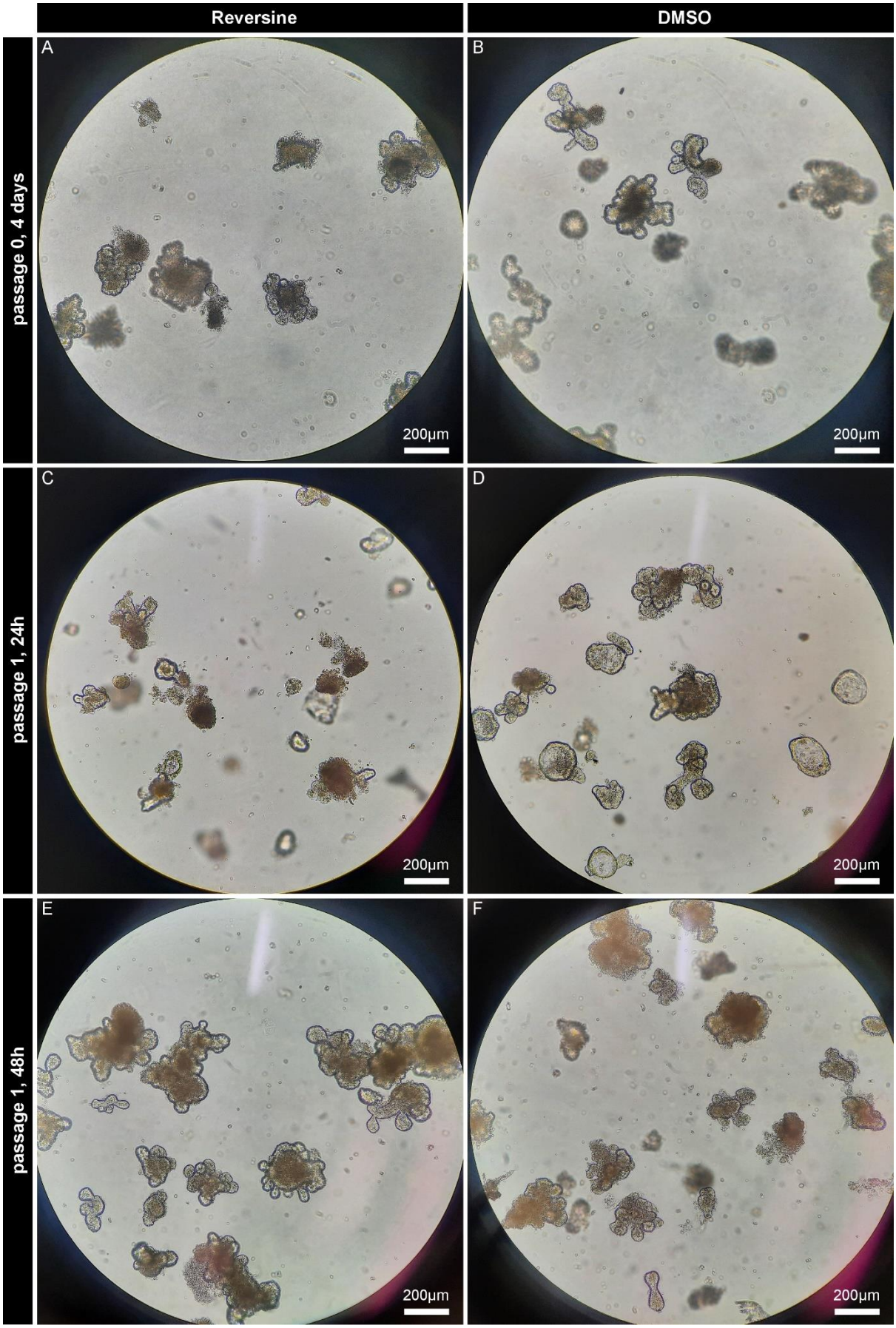
Reversine
DMSO
passage 0, 4 days
passage 1, 24h
passage 1, 48h
A
B
C
D
E
F
200µm
200µm
200µm
200µm
200µm
200µm

Supplementary Figure S2: ***Organoids treated with 125nM Reversine, followed by passaging***. ***A-B****: organoids treated for 4 days with Reversine,* ***C-D****: Reversine-treated organoids after 24h after passage,* ***E-F****: Reversine-treated organoids 48h after passage*.

Image Analysis mean grey intensity – Enteroid Monolayer

1. Images of the Monolayer were acquired using the LSM980 Confocal Microscope, 10x objective.
2. The MAX intensity projection of every slice of the stack was used: Image → Stacks → Z-Project (Figure A)
3. The image was converted to an 8-bit image (Image → Type → 8-bit) and the DAPI Channel (Figure B) was used to create a Mask (Figure D): For creating the Mask:
    a. The image needs to be thresholded: Image → Adjust→ Threshold (the Huang algorithm was used) the threshold was picked manually in a way that most nuclei were clearly visible without amplifying unspecific signal (Figure C)
    b. On the thresholded image the command Analyze → Analyze Particles was used (Parameters: Size: 25-800, circularity: 0.00-1.00, show Masks, Display result, Summarize, Add to Manager, Overlay)
4. Once the Mask was created every ROI was checked manually and if necessary, ROIs were added (Figure E)
5. The MAX intensity projection was used to extract only the channel of interest and the ROI were overlaid: Image → Overlay → From ROI manager (Figure F)
6. The mean intensity of every selected ROI was measured: ROI manager → Measure

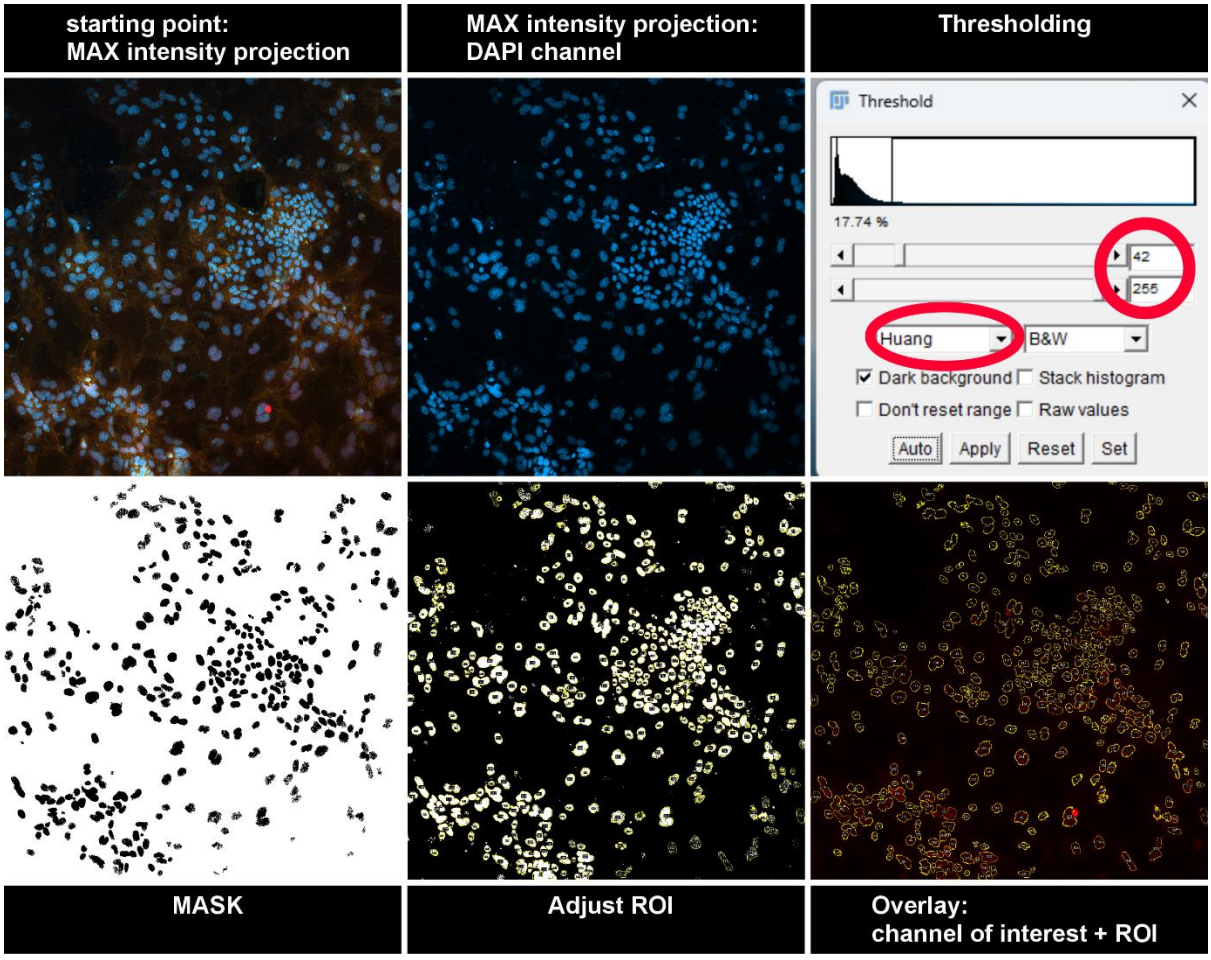

***Supplementary Figure S3**: Stepwise description of mean grey intensity value analysis.*

Exact Image processing information for mean intensity levels of p53 analysis of enteroid monolayers

Replicates	Treatment condition	Laser information	Thresholding parameters for creating the DAPI-Mask	Image information
Monolayer 2	Reversine (500nM)	Wavelength: 647 Power: 1.8%	Huang 8.98%, 19, 255	10x, MAX intensity projection of stack 1
Monolayer 2	Reversine (500nM)	Wavelength: 647 Power: 1.8%	Huang 7.55%, 8, 255	10x, MAX intensity projection of stack 2
Monolayer 2	DMSO	Wavelength: 647 Power: 2%	Huang 12.93%, 37, 255	10x, MAX intensity projection of stack 1
Monolayer 2	DMSO	Wavelength: 647 Power: 2%	Huang 11.94%, 19, 255	10x, MAX intensity projection of stack 2
Monolayer 6	Reversine (500nM)	Wavelength: 647 Power: 1.8%	Huang 17.52%, 27, 255	10x, MAX intensity projection of stack 1
Monolayer 6	Reversine (500nM)	Wavelength: 647 Power: 1.8%	Huang 6.34%, 29, 255	10x, MAX intensity projection of stack 2
Monolayer 6	DMSO	Wavelength: 647 Power: 1.8%	Huang 13.85%, 32, 255	10x, MAX intensity projection of stack 1
Monolayer 6	DMSO	Wavelength: 647 Power: 1.8%	Huang 9.36%, 37, 255	10x, MAX intensity projection of stack 2

***Supplementary Table 1:* documentation of images and their processing steps for mean intensity value quantification.** *Per treatment condition 2 technical and 2 biological replicates were used.*

Exact Image processing information for mean intensity levels of p-H2AX analysis of enteroid monolayers

Replicates	Treatment condition	Laser information	Thresholding parameters for creating the DAPI-Mask	Image information

Monolayer 2	Reversine (500nM)	Wavelength: 647 Power: 1.8%	Huang 3.36%, 30, 255	10x, MAX intensity projection of stack 1
Monolayer 2	Reversine (500nM)	Wavelength: 647 Power: 1.8%	Huang 5.33%, 37, 255	10x, MAX intensity projection of stack 2
Monolayer 2	DMSO	Wavelength: 647 Power: 2%	Huang 12.93%, 37, 255	10x, MAX intensity projection of stack 1
Monolayer 2	DMSO	Wavelength: 647 Power: 1.8%	Huang 12.32%, 37, 255	10x, MAX intensity projection of stack 2

***Supplementary Table 2*: documentation of images and their processing steps for mean intensity value quantification.** *Per treatment condition 2 technical replicates were used.*